HDPE WOOD-PLASTIC COMPOSITE

MATERIAL MODEL SUBJECT TO DAMAGE

By

GUIBIN LU

A thesis submitted in partial fulfillment of
the requirement for the degree of

MASTER OF SCIENCE IN CIVIL ENGINEERING

WASHINGTON STATE UNIVERSITY
Department of Civil & Environmental Engineering

May 2002

To the Faculty of Washington State University:

The members of the Committee appointed to examine the thesis of GUIBIN LU find it satisfactory and recommend that it be accepted.

_____

Chair

_____

_____

ACKNOWLEDGEMENT

This research project was performed at the Department of Civil and Environmental Engineering at Washington State University, Pullman, Washington. The U.S. Office of Naval Research provided funding for this research.

A number of professors have helped directly in the preparation of the research thesis.

I would like first to express my appreciation to Dr. William F. Cofer for his advice and patience while serving as my research committee chair. His thoughts on material modeling are invaluable for my study and research. The author would also like to thank Dr. John Hermanson and Dr. Balasingam Muhunthan for their advice and contributions to the research work. Dr. Hermanson provided the specimen testing data that is crucial for the material model because the constants obtained from tests were used for ABAQUS computer program. I learned fundamental knowledge of material modeling from Dr. Muhunthan 's Numerical Modeling of Geomaterials class.

The author would also like to thank Ying Du, master student Ala' Abbas and some other graduate students for their support and friendship during my academic career. Ying Du, Ala' Abbas helped me to get familiar with the ABAQUS software. We often discuss the problems related to our research. I would also like to thank graduate students Kevin Jerome Haiar and Scott Alan Lockyear for their preparing the reference information.

Finally, the author is especially grateful to his parents, and his sisters for their continued love and encouragement throughout my academic career and for the guidance they have given me in all aspects of life.

HDPE WOOD-PLASTIC COMPOSITE

MATERIAL MODEL SUBJECT TO DAMAGE

ABSTRACT

By Guibin Lu, M.S.
Washington State University
May 2002

Chair: William F. Cofer

The information presented in this thesis is part of an ongoing research project being performed at Washington State University to develop wood-plastic composite materials for waterfront structures. Material development has been finished and relevant information can be found in reference papers. Current research efforts are focused on the development of material modeling using finite element software. A two-dimensional constitutive model capable of anisotropic nonlinearity was developed to describe the hyperbolic-tangent behavior of high-density polyethylene (HDPE) composites. The main objective of this thesis is focused on the application of an approach for the spectral decomposition of the elasticity tensor to include the effect of anisotropic behavior and the use of damage concepts to model nonlinearity and failure. A homogenized continuum based on the effective stress concept was adopted for the theory of anisotropic damage and elasticity. Damage variables were introduced to describe both the evolution of the tangent stiffness and the subsequent degradation and failure of the material. Material softening was assumed to occur when the strain-state for any one of the modes from the spectral decomposition reaches a critical value. Material constants for tension and compression were obtained from uniaxial tests. Shear stiffness was obtained from a torsion test and shear damage parameters were obtained by coupling the x-direction and y-direction constants.

A user-defined material subroutine based on the material model was implemented in the Finite Element software ABAQUS to analyze and predict the behavior of the HDPE material. Based on the comparisons between the test results and predicted results from ABAQUS for simple uniaxial models, assumptions regarding the level of orthotropy of the material were adjusted. In order to evaluate the ability of the material model to accurately simulate behavior when subjected to biaxial conditions, Iosipescu and five-point bending tests were analyzed. Although displacement and strength values varied somewhat with those obtained experimentally, the mode of failure was accurately determined. With further research, the use of the concept of spectral decomposition and damage holds promise for use in general analysis of members composed of the HDPE composite material.

TABLE OF CONTENTS

LIST OF TABLES

LIST OF FIGURES

CHAPTER 1

Introduction

1.1 Background and Overview

Historically, preservative-treated wood timber has been utilized for structural elements within marine fender systems. However, as waterways have become less polluted, the traditional wood members are subjected to increasing degradation generated by marine borers. Furthermore, public concerns about water pollution in harbors have resulted in restrictions on the use of wood preservatives. As a result, an alternative material to replace the traditional wood material is required. The U.S. Office of Naval Research funded this research project with the Department of Civil and Environmental Engineering, Washington State University to investigate the feasibility of using a wood-plastic composite material (WPC) as an alternative for components of fender systems. Wood-plastic composite materials (WPC) have several benefits compared to the traditional wood material. First, it is resistant to insects, marine borers and rot when used for structural members. Without the preservative treatments, there is no environmental impact. Also, reduced production costs make wood-plastic economical for many structural applications.

The information presented in this thesis is related to two parts of the research project. One is High Density Polyethylene (HDPE) material development and the other is the use of Finite Element analysis software ABAQUS to model the nonlinear behavior of the HDPE material. The experimental testing was performed on extruded wood-based composite material, which was approximately composed of 70% wood and 30% high-density polyethylene (HDPE)

(Cofer et al., 1998). The properties of a number of wood-based composite materials have been obtained through the compression and tensile testing of specimens. Uniaxial testing has shown that wood/plastic composites display a nonlinear constitutive behavior in hyperbolic tangent form.

A simple plane stress material model for uniaxial applications was developed (Cofer, 1998, 1999), for which non-linearity from finite deformations and material behavior was included. However, that model cannot be directly applied to more general two-dimensional applications. In this thesis, a new material model is presented to describe the nonlinear behavior shown in experimental tests for plane stress applications, which is based on Continuum Damage Mechanics (CDM) and the spectral decomposition of the constitutive tensor.

1.2 The Properties and Mechanical Behavior of the HDPE Material

In this project, the high-density polyethylene (HDPE) composite material was chosen to be modeled. Specifically, the HDPE composite was composed of 58% maple flour (American Wood Fiber #4010), 31% HDPE (equistar LB0100 00), 8% inorganic filler, and 3% processing aids. For specimen tests, the HDPE material was extruded using a conical twin-screw extruder (Cincinnati-Milicron CM80) and a stranding die (Lockyear, 1999).

Tensile, compression, bending and torsion tests were performed on small HDPE composite specimens to determine its properties. Interested readers can find detailed information on experimental methods from the reports of Haiar (2000) and Lockyear (1999). Here, examples

of testing specimens are given.

Figure 1-1 shows typical extruded wood/plastic hollow test sections, which were used in uniaxial and five-point bending tests.

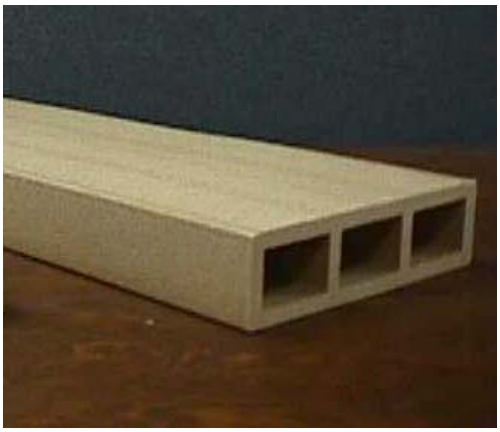

Figure 1-1: Extruded wood/plastic hollow section (Lockyear, 1999)

Figure 1-2 shows the torsion specimen. The shear modulus used as input for the HDPE model was obtained from torsion tests.

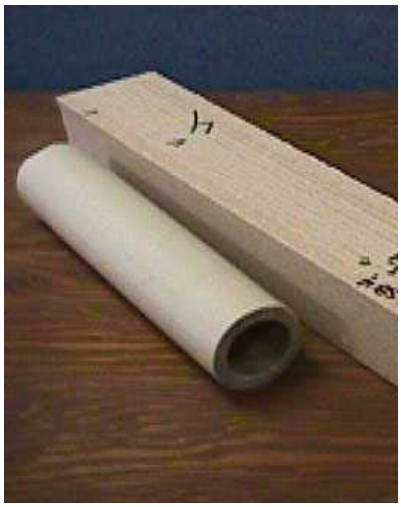

Figure 1-2: Torsion specimen (Lockyear, 1999)

Through the compression and tension tests of small specimens, the properties of the HDPE composite material have been obtained. In each case, it was found that the uniaxial stress-strain relationships are similar in shape, no matter how loads were applied. Such relationships can be represented by a hyperbolic-tangent function (Cofer, 1999):

$$\sigma = a \tanh(b\varepsilon), \tag{1.1}$$

and

$$\frac{\partial \sigma}{\partial \varepsilon} = \frac{ab}{\cosh^2(b\varepsilon)}. \tag{1.2}$$

Also, when $\varepsilon = 0$,

$$\frac{\partial \sigma}{\partial \varepsilon} = ab = MOE \text{ (Modulus of Elasticity)} \tag{1.3}$$

Here, σ and ε are uniaxial stress and strain, respectively, and a and b are constants. A typical stress-strain relationship of the HDPE material is shown in Figure 1-3, which was obtained when the load was applied in tension parallel to the material grain.

From the physical specimen tests, it was found that the HDPE composite material behaves differently in tension cases versus compression cases with respect to different values of stiffness and strength. One of the differences is the maximum strain, which is defined by the onset of softening or fracture. Table 1-1 and Table 1-2 show the tensile and compressive maximum strain values and hyperbolic tangent constitutive parameters. Another interesting phenomenon observed is that the HDPE composites are quite flexible in shear, with a shear modulus obtained from torsion tests. Table 1-3 shows the maximum strain and strength values obtained from torsion tests.

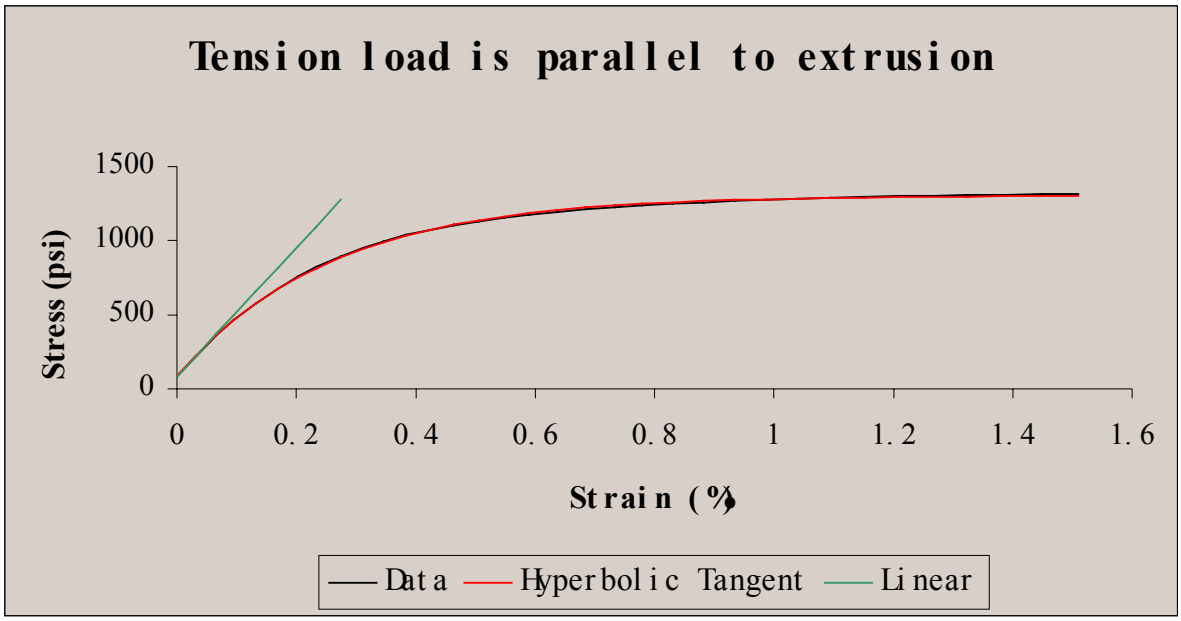

Figure 1-3:Typical stress-strain relation of the HDPE material (Lockyear, 1999)

HDPE material properties (Loading is parallel to grain)			
	ε_{max}	a	b
Tension	0.0149	1271.0	339.0
Compression	0.0459	2200.0	213.0

Table 1-1: Tensile and compressive strains and hyperbolic tangent coefficients, parallel to extrusion (Lockyear, 1999)

HDPE material properties (Loading is perpendicular to grain)			
	ε_{max}	a	b
Tension	0.00251	794.1	698.4
Compression	0.0461	2284.7	119.3

Table 1-2: Tensile and compressive strains and hyperbolic tangent coefficients, perpendicular to extrusion (Lockyear, 1999)

HDPE material properties (From torsion tests)			
	ε_{max}	Maximum Strength (psi)	Shear Modulus (psi)
Average Value	0.022	1006.3	132077.7

Table 1-3: Torsion test results (Lockyear, 1999)

1.3 Objectives

The purpose of the work of this thesis is to provide a new wood composite material model, based on concepts of damage, to extend the nonlinear behavior observed in uniaxial physical testing on the HDPE material to two-dimensional analysis. At the same time, it is necessary to evaluate the behavior related to anisotropy through the application of spectral decomposition of the constitutive tensor. Specifically, the objectives are:

1. Develop the theory of the material model.
2. Implement the model in Finite Element software and calibrate with uniaxial test data.
3. Validate its ability to accurately model biaxial behavior by modeling biaxial tests.

To realize these objectives, equivalent constitutive relations were determined, and formulations for damage evolution were developed based on Continuum Damage Mechanics and the effective stress concept. Also, some constitutive assumptions were made for this material model:

1. The HDPE material model is appropriate for plane stress conditions.

2. The stress-strain relation obtained from test data of the HDPE material is known to be nonlinear, and it appears to follow a hyperbolic tangent curve. All nonlinear effects of the constitutive behavior are attributed to damage.
3. The anisotropy of the material is represented by tensor decomposition. For the plane stress model, three eigenmodes correspond to the x-direction behavior, the y-direction behavior, and shear behavior, respectively.
4. The orientation of the eigenvectors remains unchanged after damage initializes.
5. The damage variable for the shear mode is only available through the coupling of damage variables for the normal eigenmodes.

CHAPTER 2

Literature Review

The behavior of the HDPE wood composite material is influenced by its nonlinearity and its anisotropy. The background to both is presented in this chapter.

2.1 Continuum Damage Mechanics

The analysis for the HDPE composite material subject to damage is based upon the behavior at the microscopic scale, as predicted using the concepts of effective constitutive and evolution equations (Caiazzo and Costanzo, 1999).

As Caiazzo and Costanzo indicated, "effective constitutive equations describe the behavior of a single material element of an equivalent homogeneous medium." The effective constitutive equations will vary nonlinearly during the process of loading. These equations are developed to be valid for any deformation history that a material point will experience. To obtain equations of this type is the fundamental goal of any theory of effective properties of composites. Among these theories, Continuum Damage Mechanics (CDM) and homogenization theory (HT) are the two most prominent (Caiazzo and Costanzo, 1999). In this material model, the Continuum Damage Mechanics concept was used.

Caiazzo and Costanzo defined Continuum Damage Mechanics (CDM) as "a phenomenological approach where the mathematical description of a certain type of microscopic damage mechanism is given in terms of some appropriately defined damage variables". After those variables have been determined, the constitutive relation can be obtained using continuum

thermodynamic theories of constitutive equations (Coleman and Gurtin, 1967; Coleman and Noll, 1963; Germain et al., 1983). The constitutive relation obtained will correspond to a new damage state. As the damage variables change and the properties of the nonlinearity develop, the constitutive relation will change accordingly because it is a function of those variables.

2.2 Effective Stress Concept

To develop a damage theory, the first thing is to define a damage variable because damage is not a quantity that can be measured. The theory of Continuum Damage Mechanics provides several ways to provide an equivalent homogeneous medium to describe damage, one of which is the use of the effective stress concept. Lemaitre (1983) gave a clear definition for effective stress: " A damaged volume of material under the applied stress σ shows the same strain response as the undamaged one submitted to the effective stress $\tilde{\sigma}$." In an energy sense, this definition can be explained as the energy stored in the damaged material is equivalent to the energy in a fictious undamaged material.

The damage variable can be measured through the overall section area of a material element, S, and the effective area after damage occurred, $\tilde{S}$.

$$D = \frac{S - \tilde{S}}{S}. \tag{2.1}$$

Different values of the damage variable correspond to different states of the material element.

$D = 0$ corresponds to the undamaged state;

$D = 1$ corresponds to the fully-damaged state;

$0 < D < 1$ corresponds to the damaged state.

The damage variable is used to establish the relationship between the effective (or damaged) Cauchy stress tensor $\underline{\tilde{T}}$ and the actual Cauchy stress tensor $\underline{T}$. Assuming that the load acting on the section S of the element is $\underline{F}$, the stress vector $\underline{T}$ that leads to the Cauchy stress tensor then can be obtained by $\underline{T} = \underline{F} / S$. Similarly, the effective stress vector is defined as $\underline{\tilde{T}} = \underline{F} / \tilde{S}$. Because $\tilde{S} = S(1-D)$,

$$\underline{\tilde{T}} = \underline{T} /(1-D) \ . \tag{2.2}$$

In fact, equation (2.2) avoids the calculation of $\tilde{S}$ because now the effective area can be represented by $S(1-D)$.

For anisotropic damage, equation (2.2) can be written in tensorial form as

$$\underline{\tilde{T}} = M(D) : \underline{T} \ , \tag{2.3}$$

where the symbol (:) indicates the tensorial product contracted on two indices and $M(D)$ is known as the damage effect tensor, which, in three dimensions is often defined as (Zhu and Cescotto, 1995):

$$\underline{\underline{M}} = \begin{bmatrix} \frac{1}{1-D_1} & 0 & 0 & 0 & 0 & 0 \\ 0 & \frac{1}{1-D_2} & 0 & 0 & 0 & 0 \\ 0 & 0 & \frac{1}{1-D_3} & 0 & 0 & 0 \\ 0 & 0 & 0 & \frac{1}{\sqrt{(1-D_1)(1-D_2)}} & 0 & 0 \\ 0 & 0 & 0 & 0 & \frac{1}{\sqrt{(1-D_1)(1-D_3)}} & 0 \\ 0 & 0 & 0 & 0 & 0 & \frac{1}{\sqrt{(1-D_2)(1-D_3)}} \end{bmatrix} \tag{2.4}$$

2.3 Eigentensors in Anisotropic Elasticity

As discussed in a number of reference papers (Mehrabadi and Cowin, 1990; Biegler and Mehrabadi, 1995; Arramon, et al., 1999), material models for anisotropic materials, such as wood and wood-based composites, can be defined in terms of eigenvalues and eigentensors that result from the spectral decomposition of the elasticity tensor. Here, this idea is applied to the HDPE material model. Mehrabadi and Cowin (1990) generalized the properties of elastic eigentensors:

1. For any elastic symmetry, the stress and strain tensors can be decomposed into a sum of six or fewer eigentensors of identical form.
2. For any elastic symmetry, each stress eigentensor is proportional to its strain eigentensor in identical form.
3. For any elastic symmetry, the total strain energy density may be decomposed into a sum of six or fewer terms, each term being a scalar-valued product of corresponding stress and strain eigentensors. These terms represent energy modes that are not interactive.

In order to identify the proportional stress and strain eigentensors of an anisotropic solid, a second rank stiffness tensor, $\underline{\underline{C}}$, was developed by Mehrabadi and Cowin (1990). The stress tensor is represented by $\underline{T}$ and the strain tensor is represented by $\underline{E}$. The Ath eigenvalue $\Lambda_{(A)}$ of $\underline{\underline{C}}$ satisfies the equation

$$(\underline{\underline{C}} - \Lambda_A \underline{\underline{I}})\hat{\underline{E}}^{(A)} = 0 \ , \tag{2.5}$$

where $\hat{\underline{E}}^{(A)}$ is the A th strain eigentensor and $\underline{\underline{I}}$ is the identity tensor.

From the first property stated above, the total strain is the sum of all of the eigenstrains. Similarly, the total stress can be found by summing the eigenstresses. The second property can be written for the A th eigenvalue as

$$\hat{\underline{T}}^{(A)} = \Lambda_A \hat{\underline{E}}^{(A)} . \tag{2.6}$$

The third property can be represented by

$$2\Sigma = \sum_{A=1}^{n} \hat{\underline{T}}^{(A)} \hat{\underline{E}}^{(A)} , \tag{2.7}$$

where Σ is the total strain energy density.

Again, it is noted that each of the addends of this sum quantifies an energy mode that is independent of any other terms. These non-interactive energy modes are used to set up a failure criterion taking into account anisotropy, as mentioned subsequently.

2.4 Brief Review of Past Anisotropic Material Failure Criteria

This research is developed from ideas presented by Mehrabadi and Cowin (1990), Biegler and Mehrabadi (1995), Schreyer and Zuo (1995), and Arramon, et al. (2000). The

formulation for their failure criteria is based upon the idea of the spectral decomposition of the elastic tensor into the so-called Kelvin modes. Mehrabadi and Cowin (1990) introduced the idea and defined Kelvin modes in detail.

According to their theories, the strain energy, U, is decomposed into the sum of modal energies $U^{(A)}$. After these energy modes have been defined for a given material, the limit values are determined from uniaxial tests. Biegler and Mehrabadi (1995) and Schreyer and Zuo (1995) predict that failure occurs when the energy of each mode reaches a limit value. Those failure criteria are based on Kelvin modes. Kelvin modes are actually the eigenmodes discussed previously. However, this method cannot account for the difference in material strength for tensile and compressive stress. To find a way to include the difference in tensile and compressive failure modes, Arramon, et al (2000) proposed failure criteria evaluated for positive and negative maximum eigenstress magnitudes separately.

$$2\Lambda_A U^A_{(T)} = (\sigma^{(A)}_T)^2 \text{ and } 2\Lambda_A U^A_{(C)} = (\sigma^{(A)}_C)^2. \tag{2.8}$$

Here, $\sigma^{(A)}_T$ are the tensile eigenstress magnitudes that can be determined from tests and $\sigma^{(A)}_C$ are the compressive eigenstress magnitudes that can be determined from tests. Λ_A are the eigenvalues. $U^A_{(T)}$ and $U^A_{(C)}$ are the modal energy values for tension and compression. Then the strength envelope developed from Kelvin modes is in the form:

$$(\sigma^{(A)} - \sigma^{(A)}_T)(\sigma^{(A)} - \sigma^{(A)}_C) = 0 \tag{2.9}$$

Arramon, et al. (2000) also note that, for most materials, additional modes of failure exist, which are independent of the Kelvin modes. Complementary failure modes were thus introduced, corresponding to maximum principal stress, which can be written as

$$(\sigma^{(P)} - \sigma_T^{(P)})(\sigma^{(P)} - \sigma_C^{(P)}) = 0\,, \tag{2.10}$$

Here, $\sigma_T^{(P)}$ is the maximum tensile principal stress and $\sigma_C^{(P)}$ is the minimum principal stress. They are both evaluated from multiaxial tests rather than from uniaxial test data sets. These additional modes can be called *P* modes.

The revised failure theory is the combination of stress criteria for Kelvin modes, which is related to material direction, and stress criteria for principal stress, which is related to stress direction. This can be described by

$(\sigma^{(P)} - \sigma_T^{(P)})(\sigma^{(P)} - \sigma_C^{(P)}) = 0$, and

$$(\sigma^{(A)} - \sigma_T^{(A)})(\sigma^{(A)} - \sigma_C^{(A)}) = 0\ .\ A=1,K, \tag{2.11}$$

where K= the number of Kelvin modes.

CHAPTER 3

Constitutive Relationship

Within a material model, the constitutive relationship is used to connect the stress domain with the strain domain. For the material model described here, the nonlinear stress/strain behavior is modeled through the use of damage, which represents the change in the makeup of the material. The nonlinearity and, hence, damage is assumed to initiate and evolve from the initial loading. The concept of damage is taken from the theory of Continuum Damage Mechanics, in which effective (or equivalent) stress is used to account for its effect. In this chapter, the development of the constitutive matrix within the material model is presented.

3.1 Derivation of the Constitutive relation for the HDPE Material Model (Two-dimensional)

Without the influence of damage, the constitutive law between stresses and strains is linear. This new material model is for two dimensional plane stress applications. Therefore, for two dimensional plane stress cases, the linear elastic constitutive relation between stresses and strains for orthotropic materials is well known as:

$$\underline{\sigma} = \underline{\underline{C}} \cdot \underline{\varepsilon} \tag{3.1}$$

and

$$\underline{\underline{C}} = \frac{1}{1-\upsilon_{21}\upsilon_{12}} \begin{bmatrix} E_{11} & \upsilon_{12} & 0 \\ \upsilon_{21} & E_{22} & 0 \\ 0 & 0 & (1-\upsilon_{21}\upsilon_{12})G_{12} \end{bmatrix} . \tag{3.2}$$

Like other anisotropic materials, the HDPE material behaves differently in tension, compression and shear. So this material model is assumed to be orthotropic and the initial values of E_{11} and E_{22} are obtained by averaging the tensile and compressive test data. Then v_{12} and v_{21} are assumed. In a more general case, all the coefficients of equation (3.2) could be obtained from tests.

To describe the anisotropic behavior of the HDPE material, the idea of tensor decomposition is used (Biegler and Mehrabadi, 1993 and 1995). For the two-dimensional plane stress case, the total stress $\underline{\sigma}$ and the total strain $\underline{\varepsilon}$ are decomposed into three eigentensors, which correspond to three eigenvalues accordingly. The strain eigentensor $\underline{\hat{E}}^{(A)}$ and the eigenvalues Λ_A of $\underline{\underline{C}}$ satisfy equation (2.6), as described in Chapter 2.3.

To obtain stress eigentensors and strain eigentensors, the eigenvalue equation must be solved. For convenience, $\underline{\underline{C}}$ is denoted as:

$$\underline{\underline{C}} = \begin{bmatrix} C_{11} & C_{12} & 0 \\ C_{21} & C_{22} & 0 \\ 0 & 0 & 2C_{66} \end{bmatrix} \quad . \tag{3.3}$$

Then, the equation can be rewritten as:

$$\begin{bmatrix} C_{11}-\Lambda & C_{12} & 0 \\ C_{21} & C_{22}-\Lambda & 0 \\ 0 & 0 & 2C_{66}-\Lambda \end{bmatrix} \begin{Bmatrix} E_{11} \\ E_{22} \\ \sqrt{2}E_{12} \end{Bmatrix} = \begin{Bmatrix} 0 \\ 0 \\ 0 \end{Bmatrix} \quad . \tag{3.4}$$

Mathematically, the characteristic equation is:

$$(2C_{66}-\Lambda)\left[(C_{11}-\Lambda)(C_{22}-\Lambda)-C_{12}C_{21}\right]=0\,. \tag{3.5}$$

From this equation, the roots may be obtained:

$$\Lambda_3 = 2C_{66} \tag{3.6}$$

$$\Lambda_{1,2} = \frac{1}{2}\left[C_{11} + C_{22}\right] \pm \frac{1}{2}\sqrt{C_{11}{}^2 + C_{22}{}^2 - 2C_{11}C_{22} + 4C_{12}C_{21}} \ . \tag{3.7}$$

Accordingly, the normalized eigenvectors are

$$\underline{N}_{1,2} = \left\{ \frac{\dfrac{-C_{12}}{C_{11} - \Lambda_{1,2}}}{\sqrt{\left(\dfrac{-C_{12}}{C_{11} - \Lambda_{1,2}}\right)^2 + 1}} \quad \frac{1}{\sqrt{\left(\dfrac{-C_{12}}{C_{11} - \Lambda_{1,2}}\right)^2 + 1}} \quad 0 \right\} \tag{3.8}$$

and

$$\underline{N}_3 = \left\{0 \quad 0 \quad 1\right\}. \tag{3.9}$$

From the orthogonal property of eigenvectors, the following may be defined:

$$\underline{\underline{P}}^{(1)} = \underline{N}_1^T \underline{N}_1 \tag{3.10}$$

$$\underline{\underline{P}}^{(2)} = \underline{N}_2^T \underline{N}_2 \tag{3.11}$$

$$\underline{\underline{P}}^{(3)} = \underline{N}_3^T \underline{N}_3 \tag{3.12}$$

Note that the superscript is given to distinguish different eigenmodes.

For a given total strain tensor, the strain eigentensors are defined as:

$$\underline{\hat{E}}^{(A)} = \underline{\underline{P}}^{(A)} \underline{E}\,, A = 1,3 \tag{3.13}$$

Accordingly, the stress eigentensors for elastic analysis are:

$$\underline{\hat{T}}^{(A)} = \Lambda_A \underline{\hat{E}}^{(A)}, A = 1,3 \tag{3.14}$$

Strain energy for each mode may be defined as:

$$U^{(A)} = \frac{1}{2}\underline{\hat{T}}^{(A)T}\underline{\hat{E}}^{(A)} = \frac{1}{2}\underline{\hat{E}}^{(A)T}\Lambda_A\underline{\hat{E}}^{(A)} \ . \tag{3.15}$$

According to the third property of the elastic tensor,

$$\underline{T} = \sum_{A=1}^{3} \underline{\hat{T}}^{(A)} = \sum_{A=1}^{3} \Lambda_A \underline{\hat{E}}^{(A)} = \sum_{A=1}^{3} \Lambda_A \underline{\underline{P}}^{(A)} \underline{E} \tag{3.16}$$

Therefore, the constitutive matrix is defined as:

$$\underline{\underline{C}} = \sum_{A=1}^{3} \Lambda_A \underline{\underline{P}}^{(A)} . \tag{3.17}$$

Note that this constitutive matrix is defined independently of damage. Damage variables may be introduced into this initial constitutive matrix. As described in the previous literature review, the effective stress concept is used to account for the nonlinear behavior of the HDPE wood composite material. Because damage is assumed to initialize from the very beginning, the initial constitutive matrix can no longer be applied once the loading has begun. An updated constitutive matrix corresponding to the damaged state must be used.

To define the damaged state, the plane stress stiffness tensor was decomposed into three independent eigenmodes. The assumption was made that for each of the two normal eigenmodes, there is a relevant damage variable. The two damage variables are derived based upon the uniaxial testing data, as described in the next chapter. For the shear eigenmode, a combination of damage from the normal eigenmodes is used.

According to Continuum Damage Mechanics theory, after damage occurs, the equivalent stress and strain tensors are defined for each eigenstress/eigenstrain couple as:

$$\underline{\tilde{T}}^{(A)} = \frac{1}{\left(1 - D^{(A)}\right)} \underline{\hat{T}}^{(A)} \quad , A = 1,3 \tag{3.18}$$

and $$\underline{\tilde{E}}^{(A)} = \left(1 - D^{(A)}\right) \underline{\hat{E}}^{(A)} \quad , A = 1,3 \tag{3.19}$$

Here, $\underline{\tilde{T}}^{(A)}$ is the effective (or equivalent) stress tensor and $\underline{\tilde{E}}^{(A)}$ is the effective (or equivalent) strain tensor for eigenmode A. They both can be considered to pertain to an equivalent homogeneous medium to describe the behavior of the actual damaged state. As previously noted, one of the properties of the elastic eigentensor is

$$\underline{\hat{T}}^{(A)} = \Lambda_A \underline{\hat{E}}^{(A)}, A = 1,3 \tag{3.20}$$

An assumption is made here that this property is unchanged during the damaging process. That is, the orientations of the eigenvectors do not change during loading. Then, the effective (or equivalent) stress-strain relationship is defined as:

$$\underline{\tilde{T}}^{(A)} = \Lambda_A \underline{\tilde{E}}^{(A)}, A = 1,3 \tag{3.21}$$

Which leads to

$$\underline{\hat{T}}^{(A)} = \left(1 - D^{(A)}\right)^2 \Lambda_A \underline{\hat{E}}^{(A)}, A = 1,3 \tag{3.22}$$

The effective elastic strain energy density now becomes:

$$\tilde{U}^{(A)} = \frac{1}{2}\left(1 - D^{(A)}\right)^2 \underline{\hat{E}}^{(A)T} \Lambda_A \underline{\hat{E}}^{(A)}, A = 1,3 \tag{3.23}$$

The new effective (equivalent) constitutive matrix is defined as:

$$\underline{\underline{\tilde{C}}} = \sum_{A=1}^{3} \left(1 - D^{(A)}\right)^2 \Lambda_A \underline{\underline{P}}^{(A)}, A = 1,3 \tag{3.24}$$

Chow and Lu (1989) indicated that the major hypothesis of Continuum Damage Mechanics is that energy involved in plastic flow, damaging processes, dissipated by heat, or stored in the material due to hardening are independent. In their work, the Helmholtz free energy consisted of several terms, as follows:

$$\psi^{(A)} = \frac{1}{\rho}\left[\widetilde{U}_e^{(A)} + \psi_p^{(A)} + \psi_d^{(A)}\right] \tag{3.25}$$

where $\widetilde{U}_e^{(A)}$ is the elastic strain energy, $\psi_p^{(A)}$ is the free energy due to plastic hardening, and $\psi_d^{(A)}$ is the free energy due to damage hardening. Within this material model, only elastic/damage behavior was considered.

In summary, the whole process discussed above is generalized as a flow chart, which is shown in Figure 3-1 (see next page):

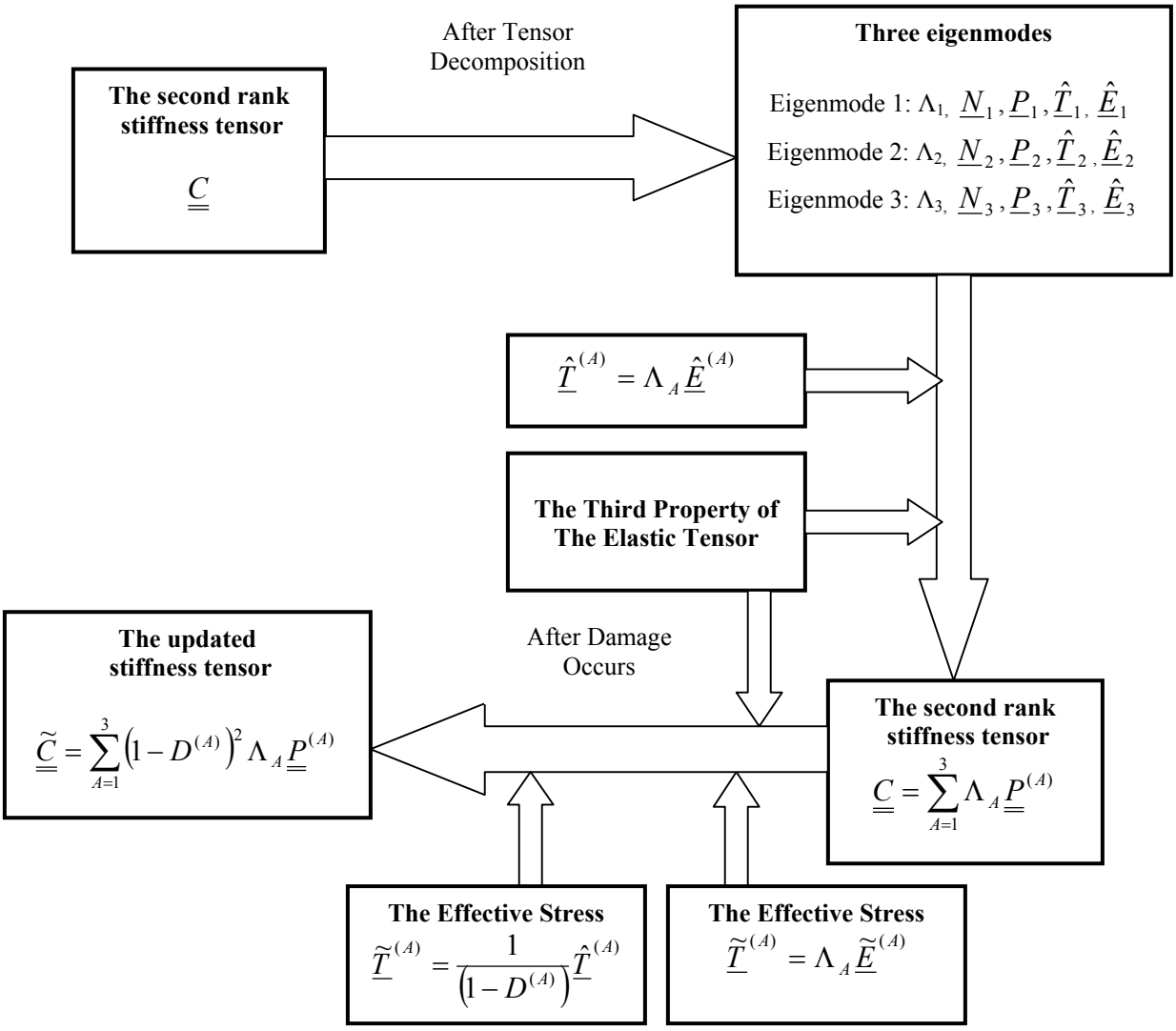

Figure 3-1: The derivation of the constitutive matrix of the HDPE material model

3.2 Summary:

In this chapter, the concept and background of Continuum Damage Mechanics were introduced. The effective stress concept, acting as a bridge between the undamaged state and damaged state, provides a way to describe the influence of damage. The idea of tensor decomposition was introduced to describe the material anisotropy. Based upon these concepts, the formulation of a constitutive relation that is valid during the nonlinear process was derived. Mathematically, the constitutive matrix obtained from the derivation is actually a function of damage variables, so that the constitutive matrix will change as damage develops.

CHAPTER 4

Characterization of Damage

For the two-dimensional model, there are three eigenmodes. The normal eigenmodes were assumed to relate to the uniaxial behavior of the HDPE material. So, the hyperbolic tangent function displayed in uniaxial behavior was applied to the two normal eigenmodes. Each eigenmode has a corresponding damage variable due to the fact that damage is a function of the magnitude of the eigenstrain. Because the assumption was made previously that damage was the cause of the nonlinearity and the hyperbolic tangent function obtained from tests shows the trend of the nonlinearity, damage of the two normal modes can be derived by taking the derivative of the hyperbolic tangent function. In addition to the normal eigenmodes, there is a shear damage mode that is the combination of the normal eigenmodes. Within an eigenmode, separate damage variables were used for tension and for compression. The constitutive matrix is looked upon as a function of damage variables, and it changes with the evolution of damage.

4.1 Definition of Damage Variables

The formulation of damage evolution is based on the hyperbolic tangent function. As indicated in the previous chapter, the uniaxial stress-strain relationship for the HDPE material follows the hyperbolic tangent curve, given in equations (1.1), (1.2) and (1.3).

Some assumptions were made for this model in Chapter 1, one of which is that the nonlinearity of the HDPE material is totally caused by damage. As is well known, the ratio of the change of stress increment and strain increment is the stiffness, and the change of the stiffness can be the measure of damage. Therefore, after taking the derivative of equation (1.2), the damage variable for uniaxial behavior has the following form:

$$D = 1 - \sec h^2\left(\frac{ab}{a}\varepsilon\right) \tag{4.1}$$

where a and b are obtained from uniaxial tests. See Table 1-1.

From the table, it is observed that the damage variable for tension must be different from that of compression no matter how the loads are applied.

Biaxial mechanical behavior can be thought of as the interaction of x-direction and y-direction uniaxial behavior. Within this material model, the idea of tensor decomposition (Biegler and Mehrabadi, 1993 and 1995) was used to describe the anisotropic properties of the HDPE material. After decomposition, three eigenmodes were obtained for the plane stress case, and each one corresponds to a specific eigenvalue. The three eigenmodes generated by the decomposition of a plane stress tensor are easily related to the x-direction uniaxial behavior, y-direction uniaxial behavior, and shear behavior for this type of directional material. Thus, each eigenmode describes one type of behavior.

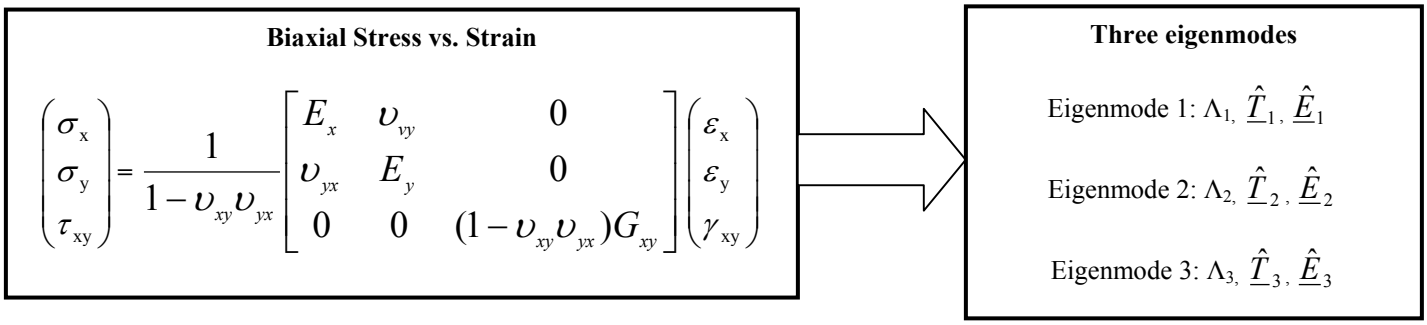

Figure 4-1: The tensor decomposition of the plane stress tensor

The uniaxial test data are available, and the damage coefficients for uniaxial tests follow the relationship of equation (4.1). They may be applied to the first two eigenmodes, having the following for damage coefficients:

$$D^{(A)} = 1 - \sec h^2\left(\frac{a^{(A)}b^{(A)}}{a^{(A)}}\varepsilon^{(A)}\right), \text{ A=1,2} \tag{4.2}$$

Note that $a^{(A)}$ were obtained from the uniaxial tests, and it can been seen that, for tension and compression, values for $a^{(A)}$ are different, so the damage variable has different values for tension and compression for the same eigenmode.

Also in equation (4.2), $\varepsilon^{(A)}$ must be a scalar measure of the strain tensor for each eigenmode because the damage variable for each eigenmode is a scalar. For each eigenmode, $\varepsilon^{(A)}$ can be represented as:

$$\varepsilon^{(A)} = (\underline{\hat{E}}^{(A)T}\,\underline{\hat{E}}^{(A)})^{\frac{1}{2}} \tag{4.3}$$

and $a^{(A)}b^{(A)}$ can be thought of as the initial elastic constant for the A-th eigenmode. Therefore, the relation between the stress eigentensor and the strain eigentensor before damage occurs can be written as:

$$\underline{\hat{T}}^{(A)} = a^{(A)} b^{(A)} \underline{\hat{E}}^{(A)} \tag{4.4}$$

According to Mehrabadi and Cowin (1990), one of the properties of the eigentensors is that each stress eigentensor is proportional to its strain eigentensor, which is represented by:

$$\underline{\hat{T}}^{(A)} = \Lambda_A \underline{\hat{E}}^{(A)} . \tag{4.5}$$

Therefore, $a^{(A)} b^{(A)}$ can be written in the form of the eigenvalue Λ_A. Equation (4.2) can then be rewritten as:

$$D^{(A)} = 1 - \sec h^2 \left(\frac{\Lambda_A}{a^{(A)}} \varepsilon^{(A)} \right) . A=1,2 \tag{4.6}$$

Within the material model, there is no independent damage for the shear mode. The reason is that, in reality, shear failure is a passive failure state. Material failure caused by shear loading results from cracks in the x-direction and y-direction. Based upon this fact, the damage variable for the shear mode is obtained by

$$D^{(S)} = 1 - \sqrt{(1 - D^{(1)})(1 - D^{(2)})} . \tag{4.7}$$

From torsion test specimens, it was also observed that the shear failure plane has a 45-degree angle with the x-z plane and the y-z plane. However, a problem arises for the pure shear case. Because strain components on material axes are zero for pure shear, $D^{(1)}$ and $D^{(2)}$ must remain zero during damage evolution, and $D^{(s)}$ must be zero. But, experimentally, the material does exhibit damage when subjected to pure shear loading. To have a non-zero shear damage parameter, shear strain is assumed to contribute equally to the damage evolution of the other two modes. The reasoning is that, with the assumption of independence of energy between the various modes, the shear strain was treated as if it acts alone. Then, the principal strains from that

pure shear case were assumed to act in tension and compression at a 45-degree angle to the 1-axis and 2-axis, causing simultaneous evolution of tensile and compressive damage.

As mentioned in Chapter 3, within the material model, only elastic/damage behavior was considered. If this idea is applied to the stress calculation, then, the equivalent eigenstress becomes,

$$\underline{\tilde{T}}^{(A)} = \rho \frac{\partial \psi^{(A)}}{\partial \hat{E}^{(A)}} = \left[\left(1 - D^{(A)}\right) \Lambda_A \underline{\hat{E}}^{(A)} \right] \tag{4.8}$$

Then, after damage occurs, for each eigenmode, the new stress-strain relations can be written as:

$$\underline{\hat{T}}^{(A)} = \left(1 - D^{(A)}\right)^2 \Lambda_A \underline{\hat{E}}^{(A)}, \; A = 1,3 \tag{4.9}$$

The equivalent eigenstress rate is

$$\dot{\underline{\hat{T}}}^{(A)} = \left(1 - D^{(A)}\right)^2 \Lambda_A \dot{\underline{\hat{E}}}^{(A)} - 2\dot{D}^{(A)} \left(1 - D^{(A)}\right) \Lambda_A \underline{\hat{E}}^{(A)} \tag{4.10}$$

Incrementally, equation (4.10) can be written as:

$$\Delta \underline{\hat{T}}^{(A)} = \left(1 - D^{(A)}\right)^2 \Lambda_A \Delta \underline{\hat{E}}^{(A)} - 2\Delta D^{(A)} \left(1 - D^{(A)}\right) \Lambda_A \underline{\hat{E}}^{(A)} \tag{4.11}$$

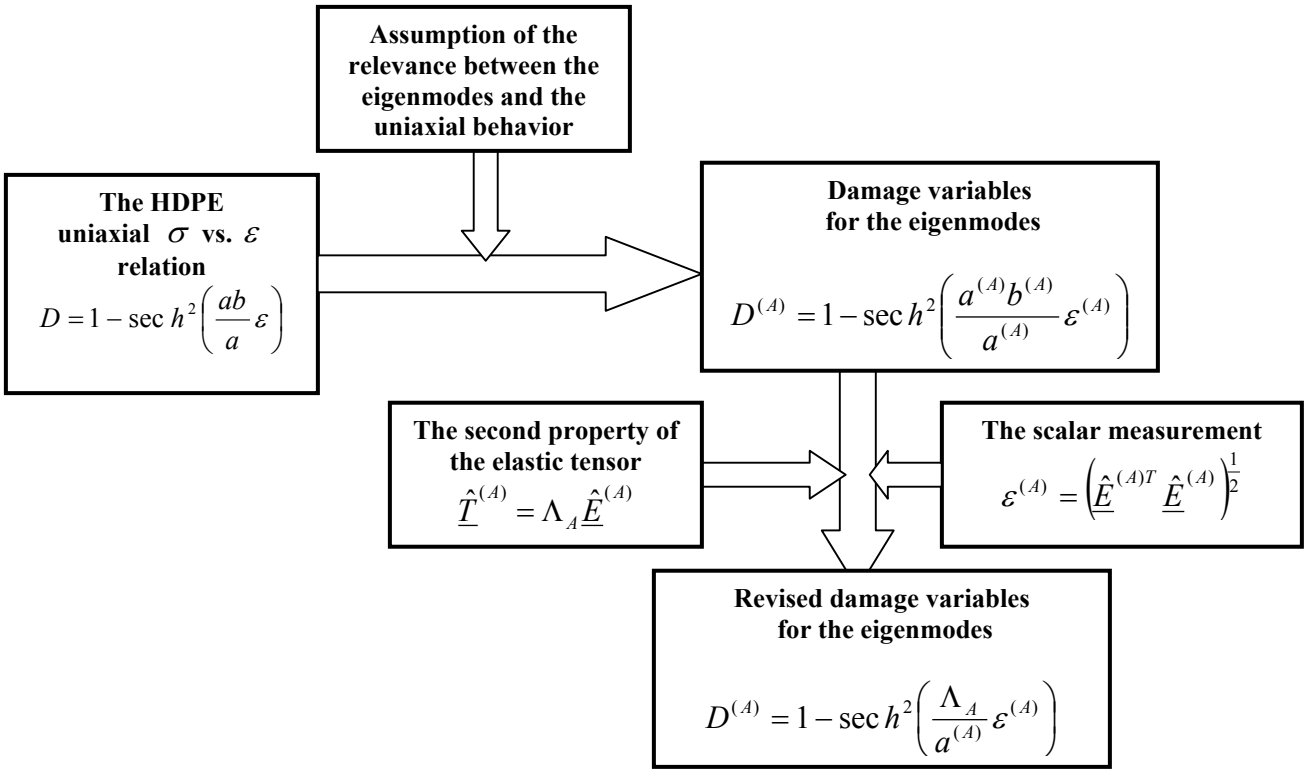

Figure 4-2: The derivation of the damage variable

4.2 Summary

In this chapter, the damage variables for the normal eigenmodes controlling the x-direction and y-direction behavior were derived. The one for the shear mode was obtained by the coupling of the damage variables for the x-direction and y-direction behavior. These derivations are based on the hyperbolic tangent function obtained from the HDPE material specimen tests.

CHAPTER 5

Uniaxial Results and Discussion

Simple finite element models with uniaxial loading were used to evaluate the basic assumptions of the proposed material model. On the basis of results, the material model was adjusted to better match observed behavior.

5.1 Damage Evolution

From tests, information is available to describe the damage evolution for the uniaxial cases. Damage variables were derived in section 4.2 and the constitutive matrix is available in Chapter 3. As an initial test, a single element model was implemented via user subroutine UMAT within the ABAQUS finite element software to describe the damage evolution of the HDPE material under uniaxial loadings. This simple model used the material constants available from the HDPE uniaxial tests, and it corresponded to a simply supported square thin block with dimensions of 20 inches x 20 inches x 2 inches. The load was applied along directions parallel and perpendicular to extrusion, which is the x-direction with the model according to the orientation. The constitutive matrix and damage variable, as previously derived, were the core part of this FORTRAN subroutine.

The following graphs show the process of damage evolution in the x-direction and y-direction. Note that the modeling of different tension and compression behavior for each mode is accomplished through the use of different damage variables.

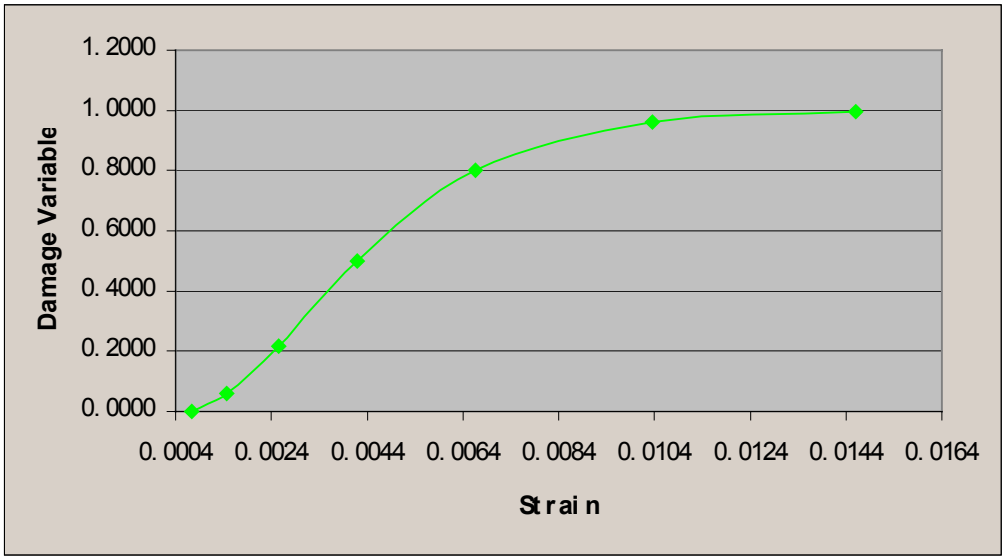

Figure 5-1: Damage evolution for the HDPE material model with uniaxial tension loading parallel to extrusion

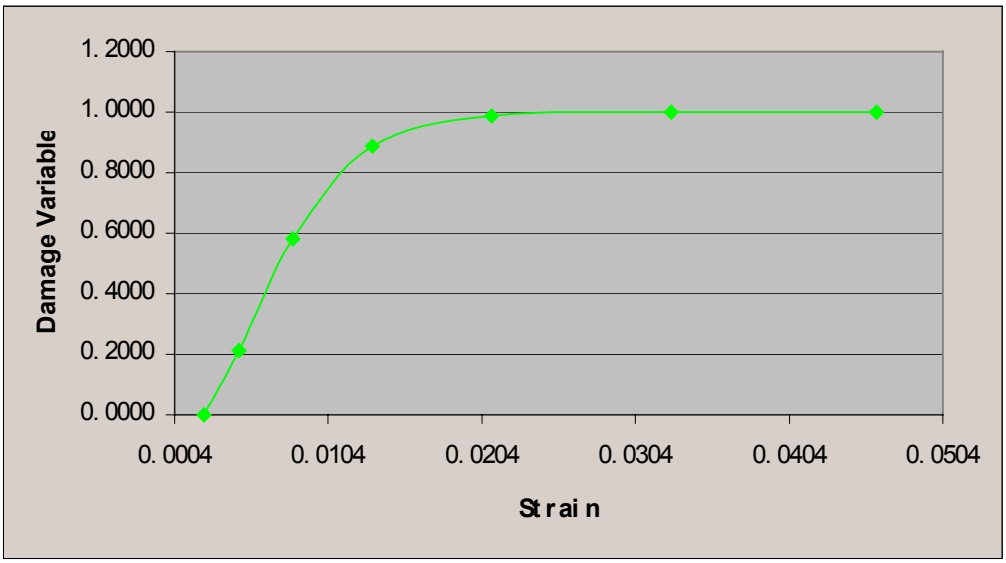

Figure 5-2: Damage evolution for the HDPE material model with uniaxial compression loading parallel to extrusion

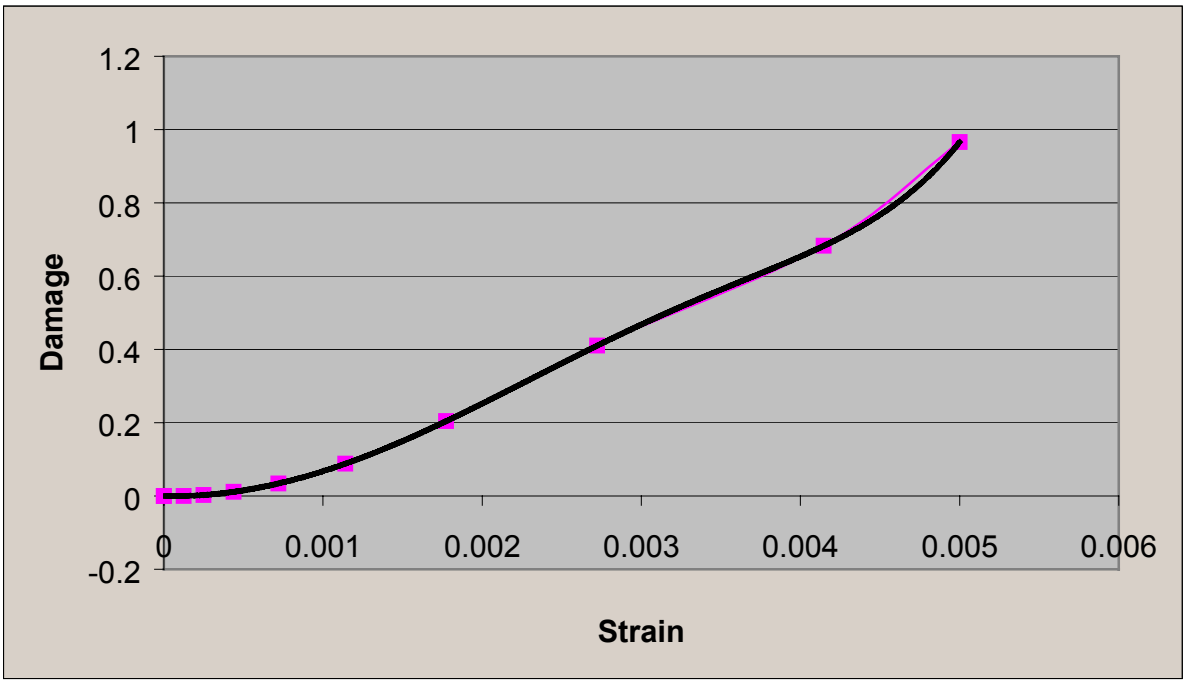

Figure 5-3: The damage and strain relation of the HDPE material model with uniaxial tension perpendicular to extrusion

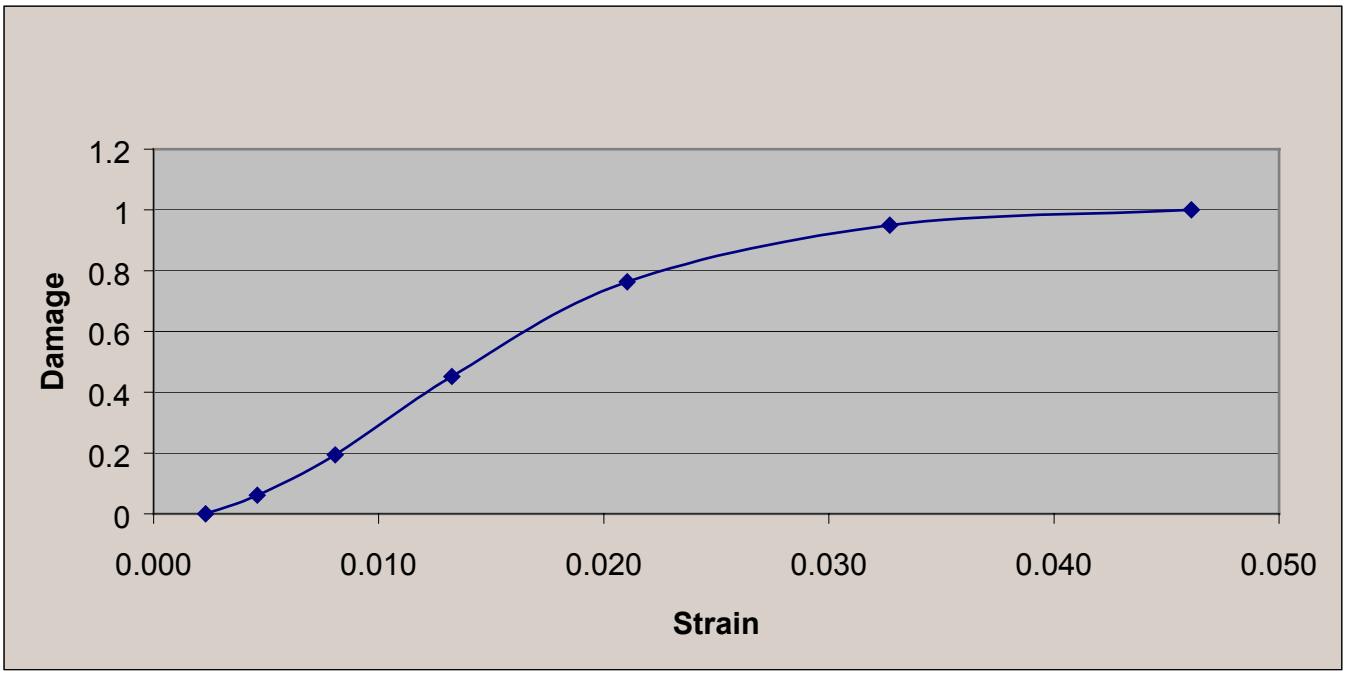

Figure 5-4: The damage and strain relation of the HDPE material model with uniaxial compression perpendicular to extrusion

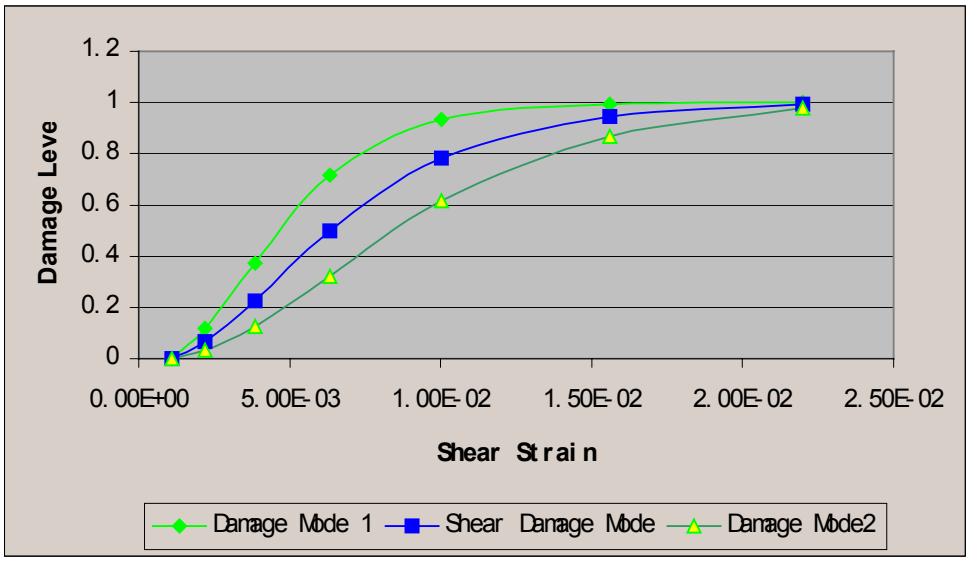

Figure 5-5: Damage evolution of pure shear case of the HDPE material model

Figures 5-1, 5-2, 5-3 and 5-4 show that damage occurs at a lower strain magnitude in tension, especially when loading is in tension perpendicular to extrusion. This phenomenon reveals that tension failure usually controls when material failure occurs. Also, these results show the material anisotropy in the x-direction and y-direction.

In Figure 5-5, it can be seen that eigenmode no.1 dominates and the damage values of the two normal eigenmodes combine to generate shear mode damage. This is due to the assumption made previously that there is no independent shear mode within the material model.

5.2 The Evolution of the Constitutive Matrix

It is always easiest to understand the nonlinearity concept from first studying a uniaxial example. For the one-dimensional case, the stress vs. strain relation of the HDPE material is

generalized as equations. Now that the material model must apply to the plane stress case, the link between the stress domain and the strain domain is no longer a variable, but a tensor. Given the constants obtained from uniaxial specimen tests, the damage evolution was described in section 4.1. From the formulations in chapter 3, it is obvious that during the nonlinear damage process the constitutive matrix of the HDPE material will vary as a result of the evolution of the damage variables. To give an example, the same user material model described in section 5.1 was used here. Note again that the single element was subjected to a uniaxial loading in the x-direction and the formulations and derivations mentioned in Chapters 3 and 4 are the fundamentals of the material model. A whole process of the evolution of the constitutive matrix accompanying the damage was then obtained, and it is shown in Appendix Tables A-9 and A-10 separately to distinguish tension and compression loading.

In these two tables, the damage variable shown is the one corresponding to eigenmode no.1, because eigenmode no.1 represents the x-direction behavior of the HDPE material in this case. Also, for tension and compression, different damage variables were used for eigenmode no.1. The damage variable which corresponds to the other normal eigenmode is irrelevant in this case. The results show that its value is too small to have a noticeable effect when the external loads are applied along the x-direction.

From the results tabulated, it is found that, during the nonlinear damage process, the constitutive matrix changes its components. If the external loading is parallel to extrusion, which was defined as the x-direction in the ABAQUS UMAT subroutine, C_{11} experienced larger changes compared to C_{22}. This phenomenon is due to the fact that, within this model, the

damage variables $D^{(1)}$ and $D^{(2)}$ correspond to the normal eigenmodes, respectively. The eigenmode one is related to the x-direction behavior, and the eigenmode two is related to the y-direction behavior. The tabulated results reflect the x-direction behavior which is dominated by $D^{(1)}$. C_{11} is a function of $D^{(1)}$, so from the table, it is observed that C_{11} controls the changes.

Although the results of loading in the y-direction are not listed, it can be concluded that if the external loading is perpendicular to the grain, which is y-direction in the ABAQUS model, changes in C_{22} will dominate the change in properties with respect to C_{11}.

5.3 Uniaxial Behavior Modeling

This material model was calibrated with the uniaxial test results. To get the uniaxial stress vs. strain relations, the same user material model described in section 5.1 was used. Again, the formulations and derivations mentioned in Chapters 3 and 4 are the fundamentals of the material model. The results are shown in Figure 5-6, labeled as the "CDM result". From the figure, the results do not match those of experiment in that the response indicates abrupt softening, followed by a leveling off. For the case of tension parallel to extrusion, stress in the test specimen rises rapidly with strain and then levels off in a region that appears plastic in its behavior. Thus, the material model, as derived in Chapter 4 on the basis of the theory of Continuum Damage Mechanics, does not exhibit the apparent plastic behavior observed in the tests. One may observe that the growth of damage causes a reduction in both tangent stiffness and existing stress. The latter causes strain softening, which does not allow for the stress plateau

that was observed experimentally. To better model the experimental behavior, the model was adjusted in two ways.

First, to represent the apparent plastic behavior, the term representing the reduction in existing stress was removed. Essentially, given the definition of damage evolution that was used, this simply ensures that the stress-strain relationship follows the hyperbolic tangent curve by using the tangent stiffness. Then, a second set of damage parameters was introduced to replace the terms removed and cause softening, but only after a critical value of strain has been reached. Thus, for each eigenmode, A,

$$\Delta\underline{\hat{T}}^{(A)} = \left(1 - D^{(A)}\right)^2 \Lambda_A \Delta\underline{\hat{E}}^{(A)}, A=1, 2, 3 \tag{5.1}$$

if $\varepsilon^{(A)} < \varepsilon^{(\mathrm{A})}_{damage}$, where $\varepsilon^{(\mathrm{A})}_{damage}$ is the strain level at which softening begins. If $\varepsilon^{(A)} \geq \varepsilon^{(\mathrm{A})}_{damage}$,

$$\Delta\underline{\hat{T}}^{(A)} = \left(1 - D^{(A)}\right)^2 \Lambda_A \Delta\underline{\hat{E}}^{(A)} - \Delta D_2^{(A)} \underline{\hat{T}}^{(A)}. \tag{5.2}$$

$D_2^{(A)}$ are the softening damage parameters which are initially set to zero. When $\varepsilon^{(A)} \geq \varepsilon^{(\mathrm{A})}_{damage}$, $D_2^{(A)}$ is set to increase linearly to a value of 1.0 for $\varepsilon^{(A)} = \varepsilon^{(A)}_{\lim it}$. Thus, the stress-strain relationship follows the hyperbolic tangent curve until the damage strain is reached, at which point softening begins. The rate of softening is dictated by the limit strain, $\varepsilon^{(A)}_{\lim it}$, specified here as a multiple of the damage strain. The results for the case of tension parallel to extrusion are shown in Figure 5-6, labeled as "HDPE model".

From the stress-strain relations shown in Figures 5-6, 5-7 and 5-9, it is shown that for compression, parallel and perpendicular to extrusion, the stress-strain relationships are similar in shape to that of tension parallel to extrusion except that they are more gradual and experience crushing rather than fracture. For tension perpendicular to extrusion, the material behaves in a

brittle manner. The stress-strain relationship matches the hyperbolic tangent function only until failure occurs suddenly at a relatively low strain value. In Figure 5-8, the experimental and numerical results are somewhat different. The experimental data and the values of the constants, *a* and *b*, were taken from past work (Lockyear, 2000). Close inspection of the experimental data shows that, in all cases for tension perpendicular to extrusion, specimens were initially subjected to compressive force before being loaded in tension. In Figure 5-8, the experimental points have been shifted horizontally to approximately pass through the origin and the negative points have been discarded. However, the curve that was fit to the data does not take into account the vertical shift and, thus, appears to be somewhat high. Modification of existing constants was beyond the scope of this work, however.

Figures 5-6 through 5-9 show softening behavior in the material. However, the curves in Figure 5-7 require explanation. If the specimen is free to expand, the lateral strain, perpendicular to extrusion, attains failure during compressive loading parallel to extrusion. If expansion is restrained, softening failure results from material crushing. For the direction perpendicular to extrusion, tensile softening properties were set from both previously mentioned tests (labeled as orthotropic damage) and from the assumption that they are the same as those parallel to extrusion, for reasons described subsequently. The actual test specimen was a relatively large extruded section with a complicated pattern of lateral restraint, which eventually exhibited brittle failure. This type of complex behavior could not be simulated well with a single-element model.

Table 5-1 shows the damage strain magnitude related to each eigenmode. These values were obtained from uniaxial tests. Failure data for all of the tests were predictable and repeatable except for those in tension perpendicular to extrusion, as given in Table 5-2. Because of the large

amount of scatter in the data, average values for only cases T90^o-2, T90^o-3, T90^o-4, and T90^o-5 were used.

	Damage strain
Uniaxial tension parallel to grain	0.0146
Uniaxial compression parallel to grain	0.0459
Uniaxial tension perpendicular to grain	0.00255
Uniaxial compression perpendicular to grain	0.0461

Table 5-1: The damage strain related to eigenmodes

Specimen No.	Constant a	Constant b	Damage strain
T90°-1	1534	250	0.0023630
T90°-2	855	639	0.0026570
T90°-3	763	703	0.0022950
T90°-4	672	854	0.0020810
T90°-5	885	595	0.0031540
T90°-6	456	1190	0.0016910
Average Values Used	794	699	0.002547
Standard Derivation	42.30%	43.93%	21.04%

Table 5-2: Test data with uniaxial loading perpendicular to the grain (Lockyear, 1999)

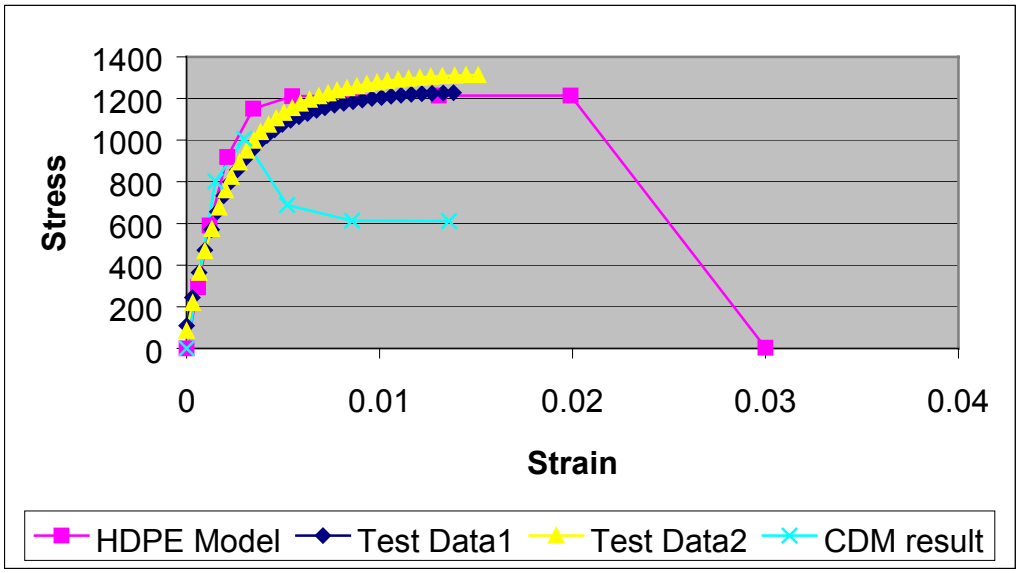

Figure 5-6: The stress and strain relation of the HDPE material model with uniaxial tension parallel to extrusion.

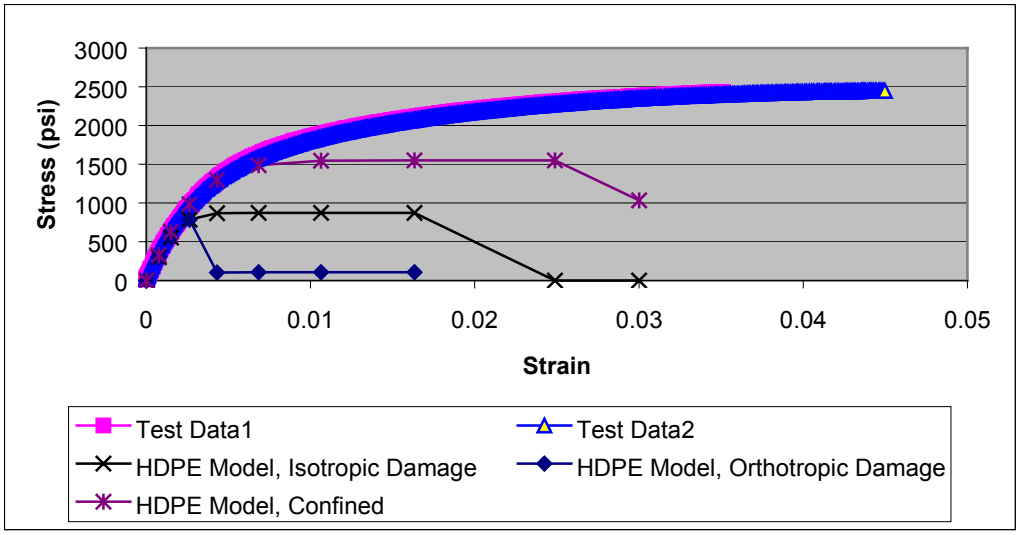

Figure 5-7: The stress and strain relation of the HDPE material model with uniaxial compression parallel to extrusion.

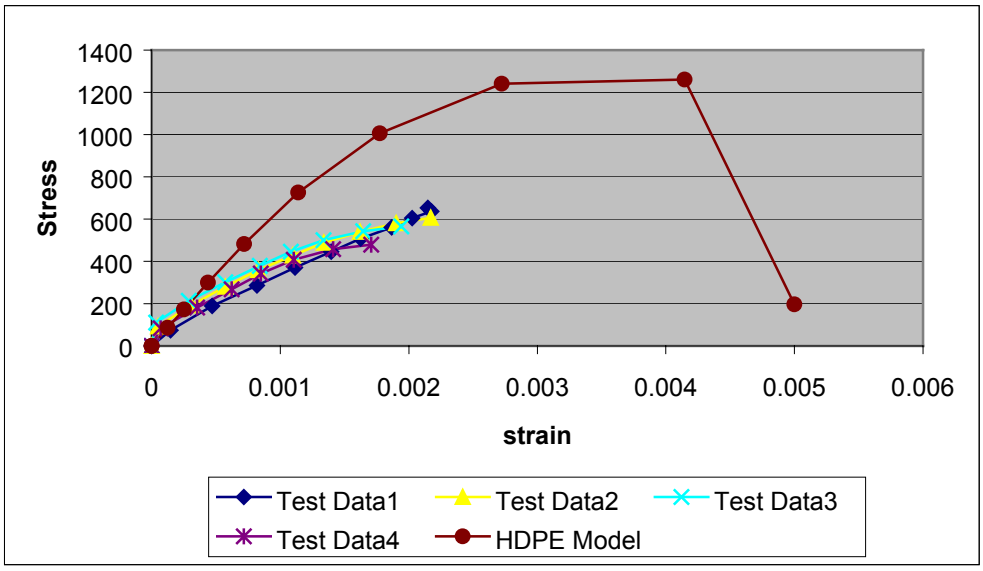

Figure 5-8: The stress and strain relation of the HDPE material model with uniaxial tension perpendicular to extrusion

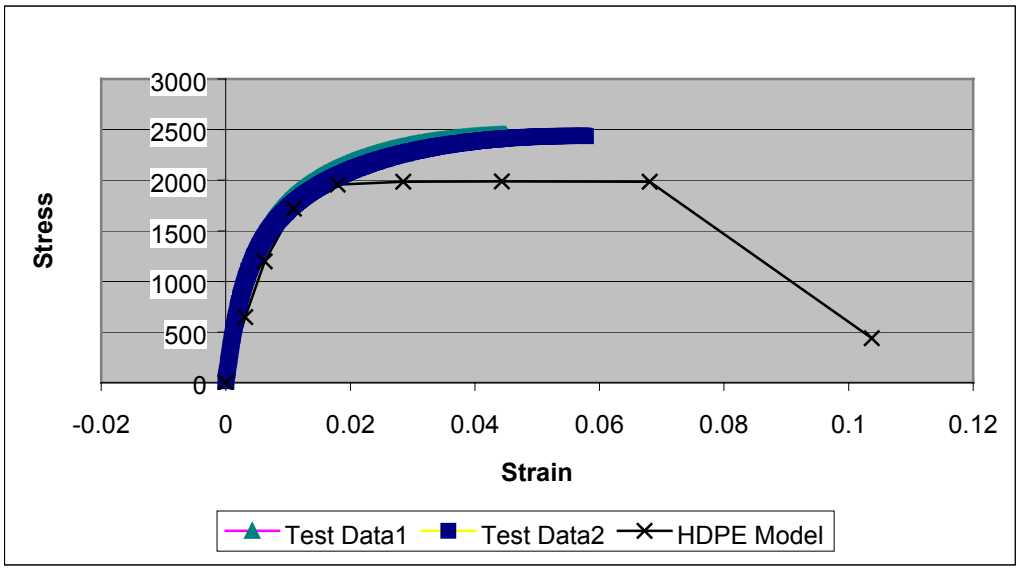

Figure 5-9: The stress and strain relation of the HDPE material model with uniaxial compression perpendicular to extrusion.

Stress level when maximum strain is reached			
	Stress (ABAQUS)	Stress (Test)	Difference/Avg (%)
Uniaxial tension parallel to extrusion	1214	1277	5.06%
Uniaxial compression parallel to extrusion	1550	2434	36.32%
Uniaxial tension perpendicular to extrusion	1171	597	64.93%
Uniaxial compression perpendicular to extrusion	1987	2284	13.90%

Table 5-3: Comparison of the results for the material model with uniaxial tests

Maximum stress data is listed in Table 5-3. The stress attained in the model is reasonably close to experimental values except for the compression parallel to extrusion and tension perpendicular to extrusion cases, as discussed earlier. The differences are likely caused by the fact that the directions of the eigenmodes matched only approximately the direction of extrusion.

It also can be observed from the stress-strain relationship that the finite element model has approximately the same initial stiffness as that of the real material, which implies that the eigenvalues and the eigentensors used within the material model are reasonable.

5.4 Shear Behavior Modeling

As discussed in Chapter 4, within the material model, damage for the shear mode is obtained by combining damage from the two normal eigenmodes. Under pure shear loading, the shear mode also contributes to the damage evolution of the normal modes. Torsion tests provide pure shear test data for the verification of the material model. Figure 1-2 shows the torsion test

specimen. A single-element model, shown in Figure 5-10, was used to model the shear behavior. In it, the y-direction displacement on top and all the displacements at the bottom were constrained, so it creates a pure shear case.

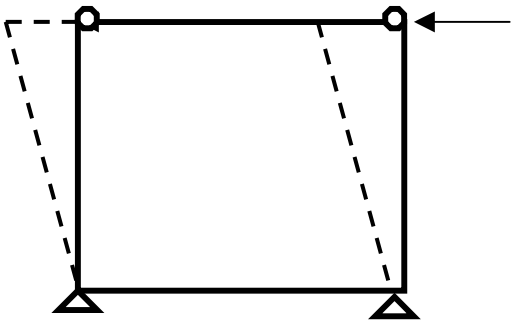

Figure 5-10: The single-element HDPE material model used for modeling torsion tests.

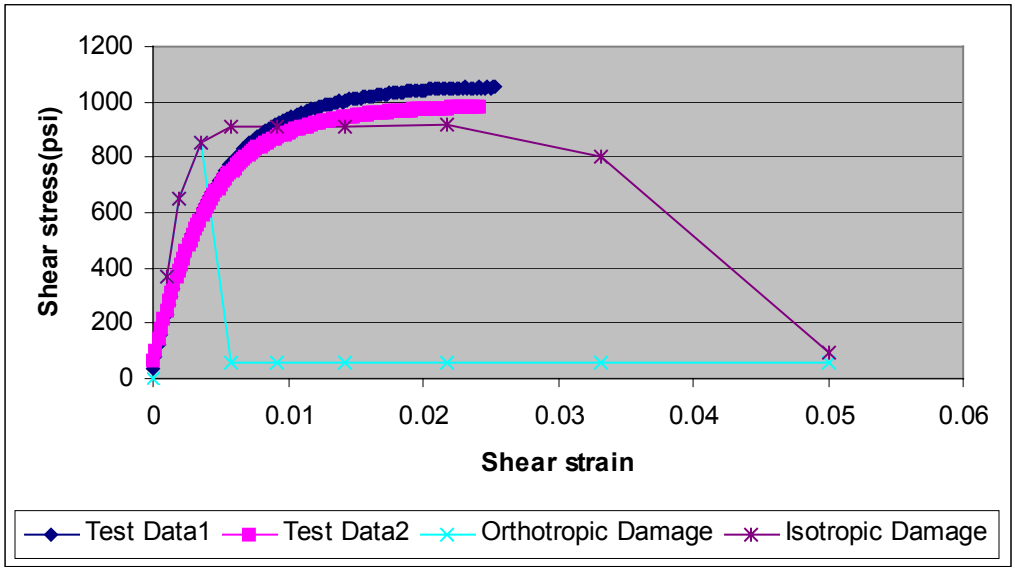

Figure 5-11: Comparison of the pure shear results for the HDPE material model with torsion tests

Maximum stress level when maximum strain is reached (psi)			
	Stress (ABAQUS)	Stress (Torsion Test)	Difference/Avg (%)
Pure Shear	914	1006	9.15%

Table 5-4: Comparison of the max shear stress for the HDPE material model and torsion tests

From Figure 5-11, the experimental and numerical curves are quite different when the given uniaxial data is used. The softening/failure shown in the model at such an early stage in the analysis is caused by the assumed brittleness of the material when subjected to tension perpendicular to extrusion, labeled as the Orthotropic Damage case. However, experimental observations indicated failure by fracture on planes of 45 degrees. The experimental behavior is inconsistent with the assumption of the weak/brittle plane perpendicular to extrusion that was assumed in the model. If the weakness is removed and the tension properties are assumed to be the same both parallel and perpendicular to extrusion, labeled as the Isotropic Damage case, the experimental and numerical curves are similar. The early fracture failure from analyses of both the torsion test and the compression test parallel to extrusion point out the inconsistency between the tension tests perpendicular to extrusion and the others. Further tests should be conducted to reconcile these differences, but testing is beyond the scope of this work.

5.5 Summary

In this chapter, the method of considering damage was modified to better reproduce experimental behavior. Material softening was considered. The revised approach was shown to be reasonably accurate for uniaxial loading and real material behavior, except when the response was dominated by damage/fracture perpendicular to extrusion.

CHAPTER 6

Biaxial Results and Discussion

The proposed material model has been shown to reasonably reproduce the behavior of the HDPE material for uniaxial loading. One of the objectives of this research is to determine how the material model presented in this thesis performs for more general applications. The Iosipescu and Five-point bending tests provided some biaxial data with which the material model could be compared.

6.1 Iosipescu Shear Test

The Iosipescu shear test (ASTM D5379) is a standard test to determine the shear strength of materials. Figure 6-1 shows the test setup for the Iosipescu test. The test fixture consists of two parts that clamp the specimen. Load is applied to one of the parts, which is allowed to slide vertically, enforcing shear in the notch of the specimen. Detailed descriptions of this test can be found in ASTM D 5379 and the report of Haiar (2000).

Figure 6-2 shows the Iosipescu test model with boundary conditions within ABAQUS finite element software. The specimen is a 3 inch x 0.75 inch x 0.3 inch block with a 90- degree notch on each edge. Specific dimensions and boundary conditions can be found in ASTM D5379 (1998). For the finite element model, nodes representing the surfaces of the specimen subject to load from the fixture were constrained to move vertically.

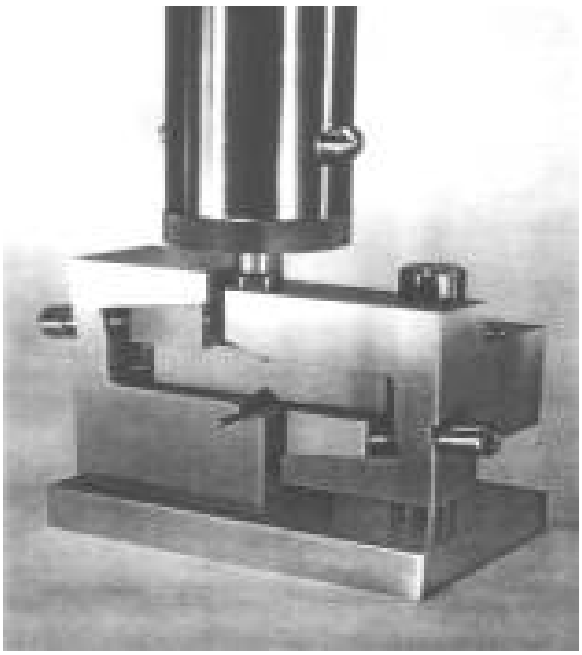

Figure 6-1: Iosipescu shear test setup

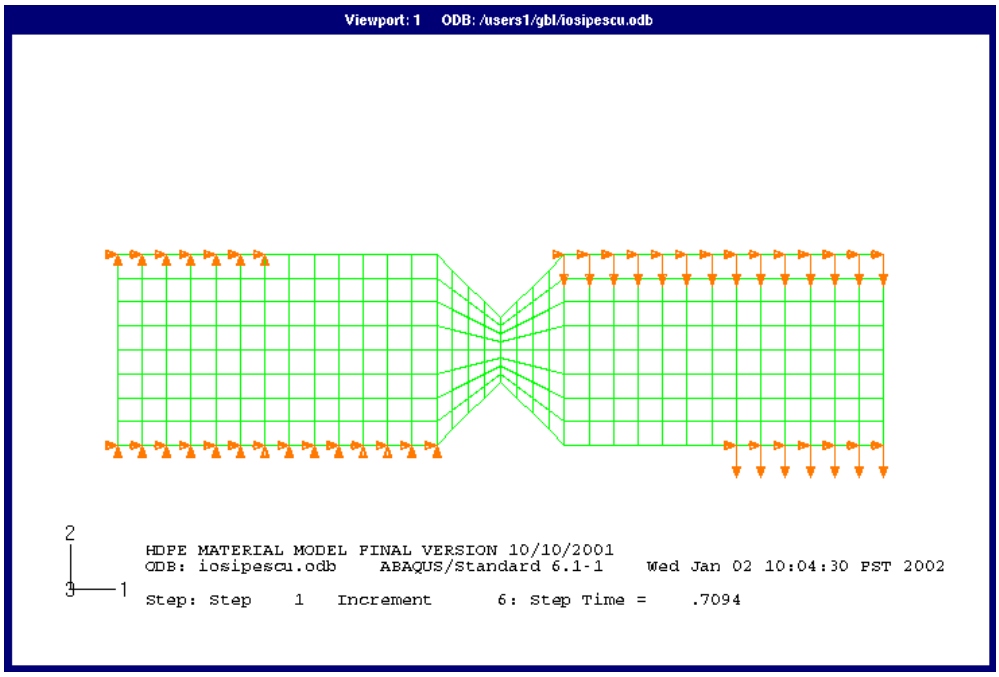

Figure 6-2: The Iosipescu shear test model with ABAQUS

For this model, cases for both orthotropic damage (i.e., weak in tension perpendicular to extrusion) and isotropic damage were considered. Load and deflection data, as well as softening damage and strain were examined. Load versus deflection data are shown in Figure 6-3. It is observed from the figure that, when failure occurs, the Iosipescu model achieves a maximum strength level that is close to that of test results for both cases. The maximum strength results are tabulated in Table 6-1. The load-deflection relationship shows material softening, with a reduced failure strength for the orthotropic damage case compared to that of the isotropic damage case.

The load-deflection result of the Iosipescu specimen analysis shows that the finite element model is very stiff compared with the test, even at the very beginning of the analysis. However, in the uniaxial analyses of the previous chapter, the stiffness of the model agreed quite well with test results, especially in the early stages of loading. Therefore, one may speculate that the large difference in displacement data is the result of a lack of agreement in the items being compared, such as additional effects of flexibility in the test fixture or local deformation in the specimen. Indeed, the Iosipescu test setup is relatively complex, while the finite element model was simple.

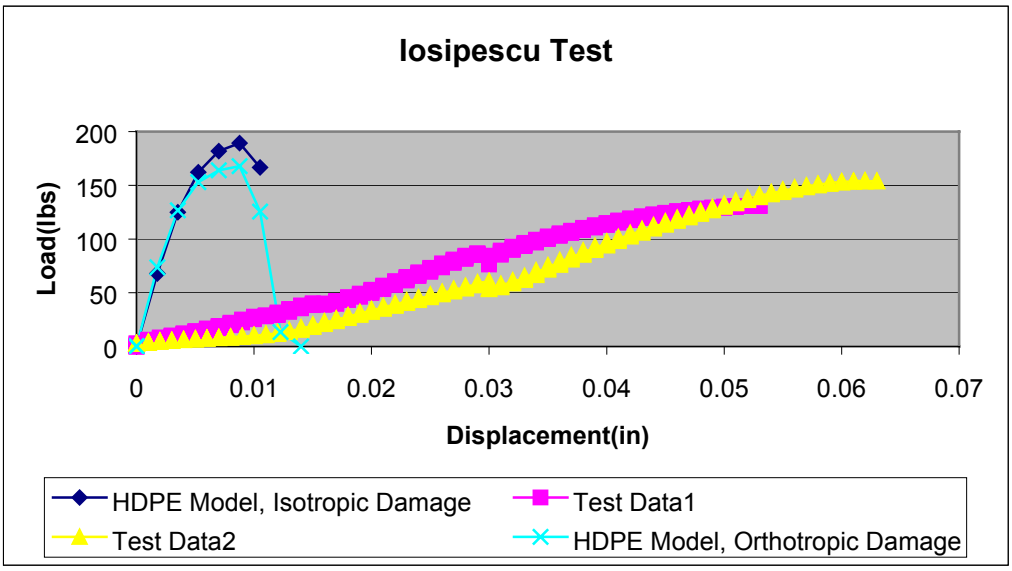

Figure 6-3: Comparison of the load-deflection relation for the Iosipescu test and the HDPE material model

Figures 6-4 through 6-6 show the damage for the normal and shear modes after the onset of material softening for the case with orthotropic damage. Failure initiates at the root of the notches and appears to propagate in a biased way toward the lower right and the upper left. As expected, failure is dominated by the assumed weakness in the material perpendicular to extrusion. Similar results are shown for the isotropic damage case in Figures 6-7 through 6-9. Damage is more concentrated at the root of the notch for the case of isotropic damage versus the case of orthotropic damage.

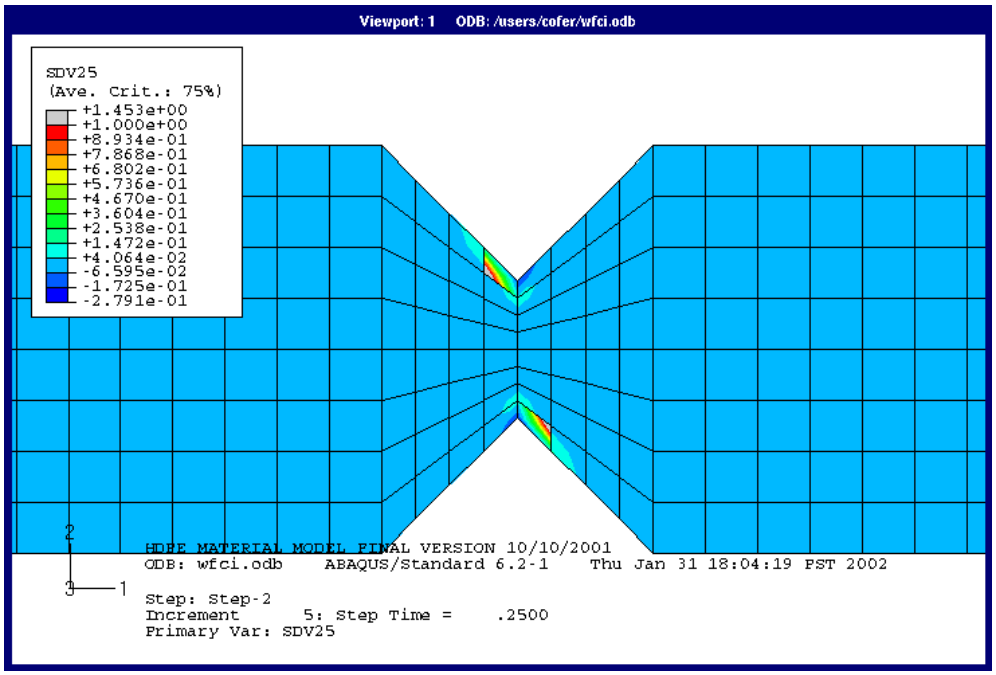

Figure 6-4: Softening damage parameter for mode 1 with orthotropic damage properties

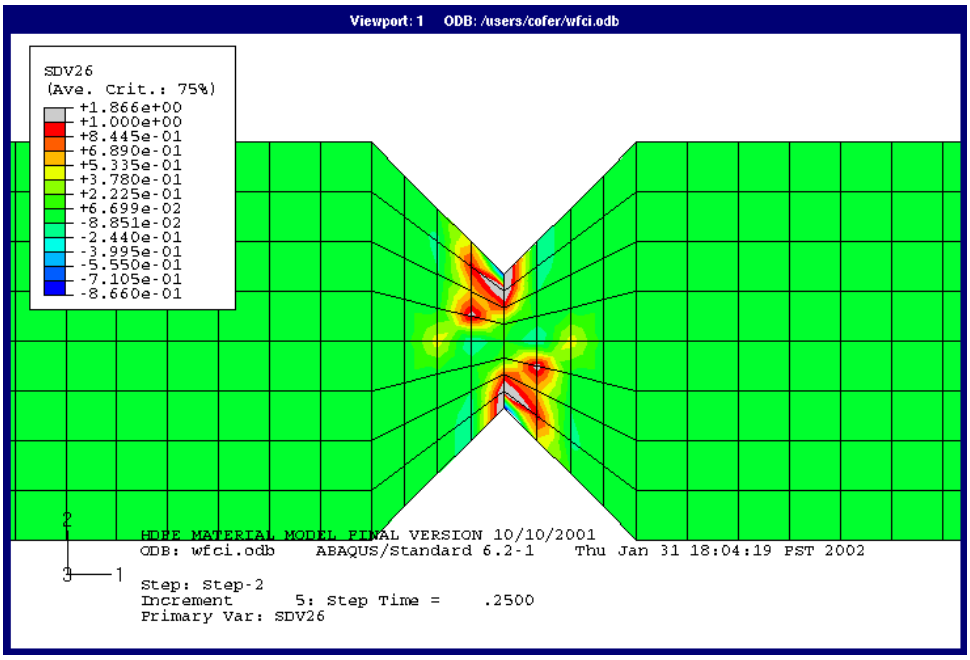

Figure 6-5: Softening damage parameter for mode 2 with orthotropic damage properties

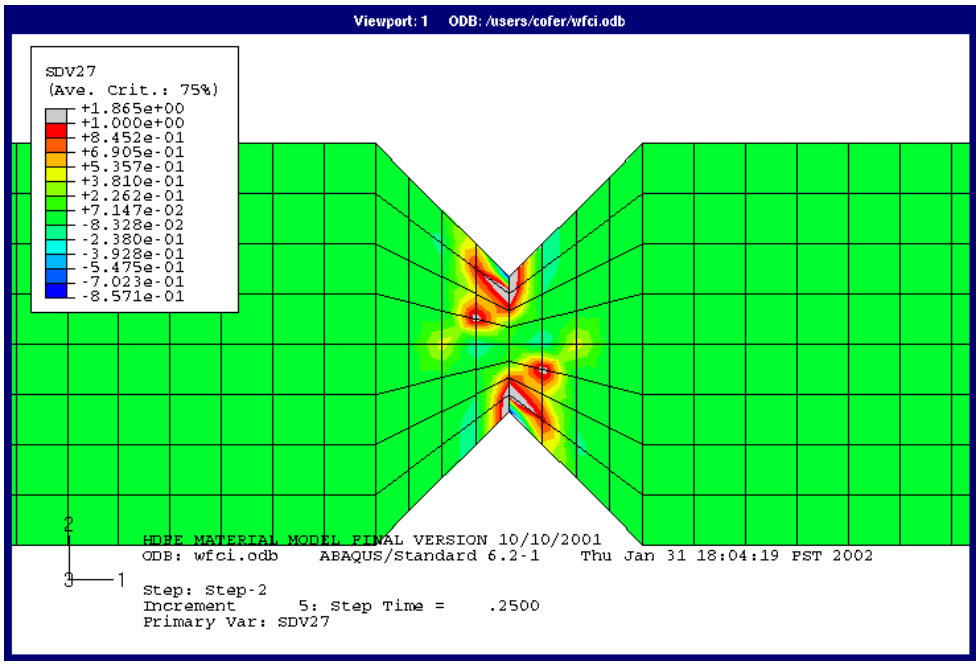

Figure 6-6: Softening damage parameter for shear with orthotropic damage properties

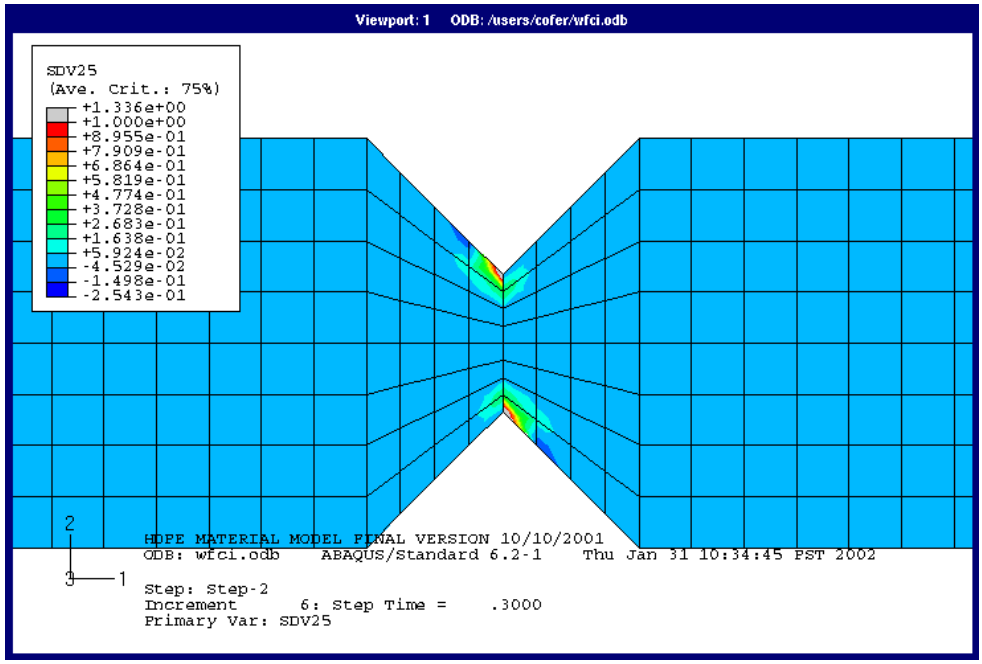

Figure 6-7: Softening damage parameter for mode 1 with isotropic damage properties

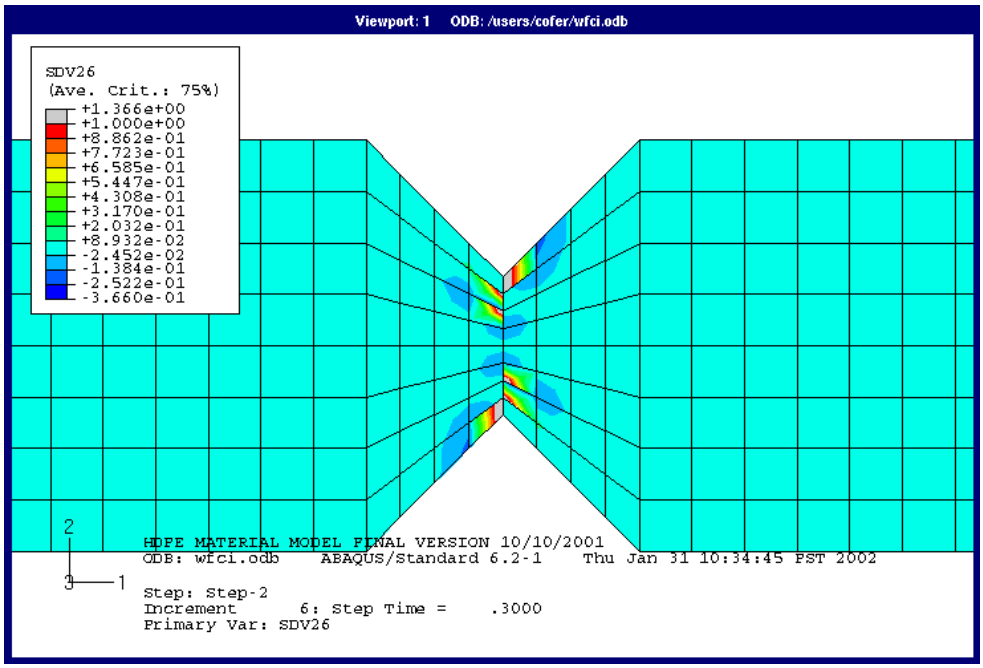

Figure 6-8: Softening damage parameter for mode 2 with isotropic damage properties

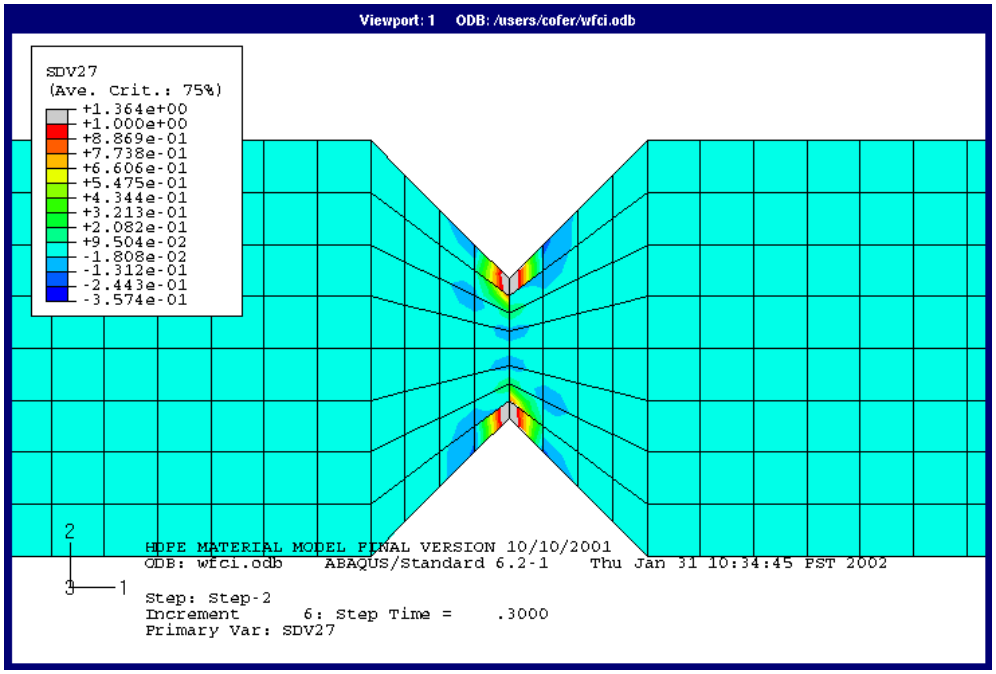

Figure 6-9: Softening damage parameter for shear with isotropic damage properties

Figures 6-10 and 6-11 show the principal strain pattern for the Iosipescu model with orthotropic damage properties at the point of maximum strength and at failure, respectively. The red arrows denote maximum tensile strain while the yellow arrows show maximum compressive strain. Prior to softening, shown in Figure 6-10, the strain is concentrated in the region between the notches and, in that location, it is primarily shear strain. After softening, shown in Figure 6-11, the strain becomes highly concentrated. One may note that the strain values shown in Figure 6-11 are much greater than those of Figure 6-10. Because the large strains occur in elements subject to damage and softening, their values may be unreliable. However, the maximum tensile strains occur at the root of the notches, oriented at an angle of 45 degrees, and they are nearly uniaxial. Away from the root of the notches, the tensile strains are oriented vertically with corresponding horizontal compressive strains, indicating shear.

Principal strain for the last three steps of the analysis of the Iosepescu model with isotropic damage properties is shown in Figures 6-12 through 6-14. Figure 6-12 represents the step prior to that of maximum strength. As with the case of orthotropic damage properties, the strain is concentrated between the notches, and it is dominated by shear. In Figure 6-13, representing the state of maximum strength, high strain has begun to localize. The strain state at softening is shown in Figure 6-14.

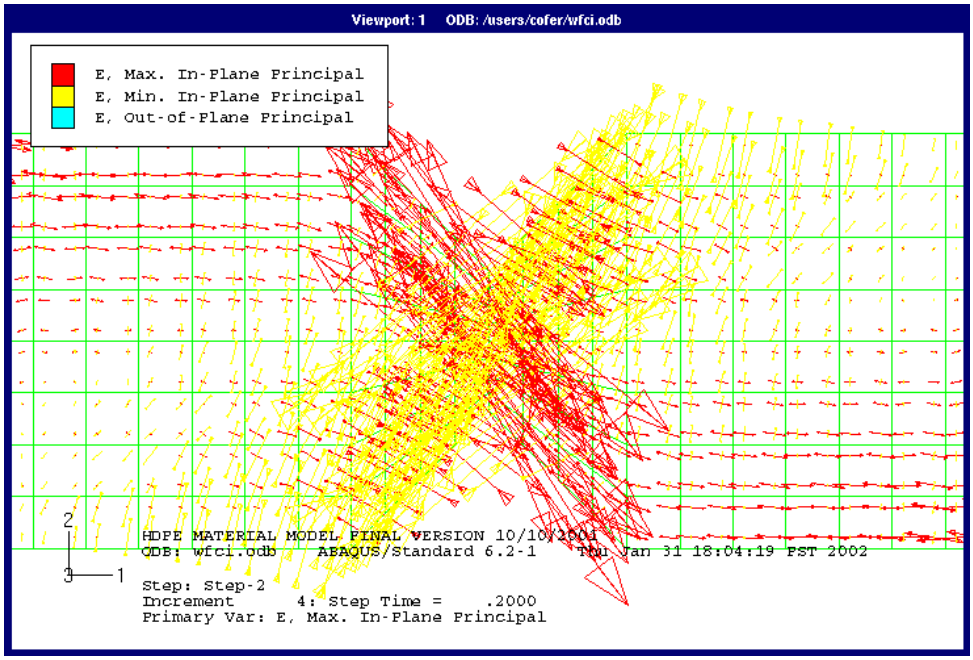

Figure 6-10: Principal strain at maximum strength with orthotropic damage properties

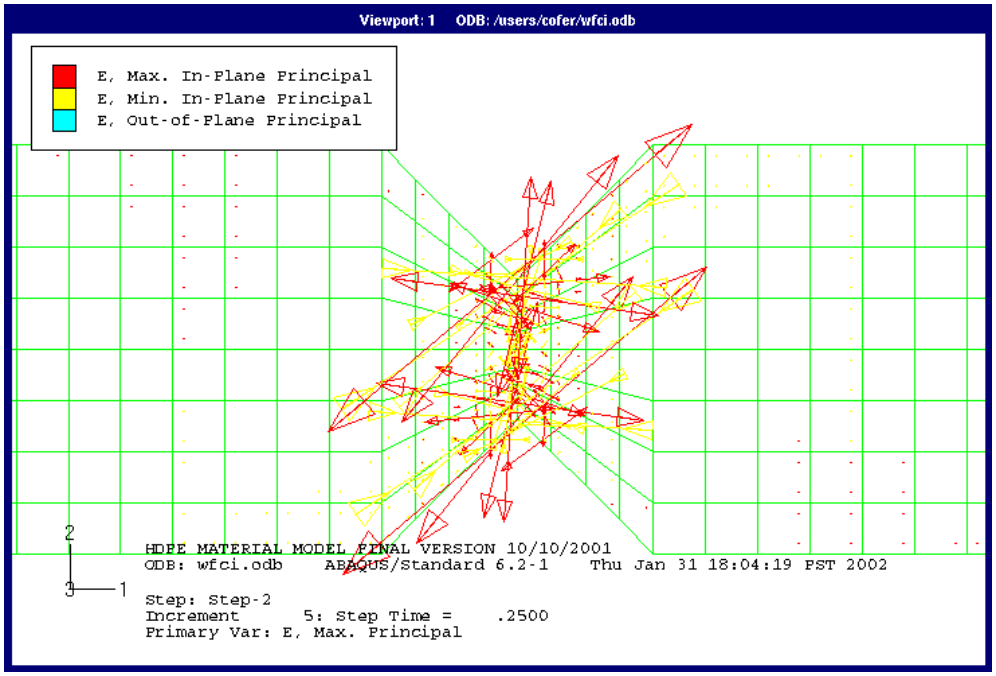

Figure 6-11: Principal strain at failure with orthotropic damage properties

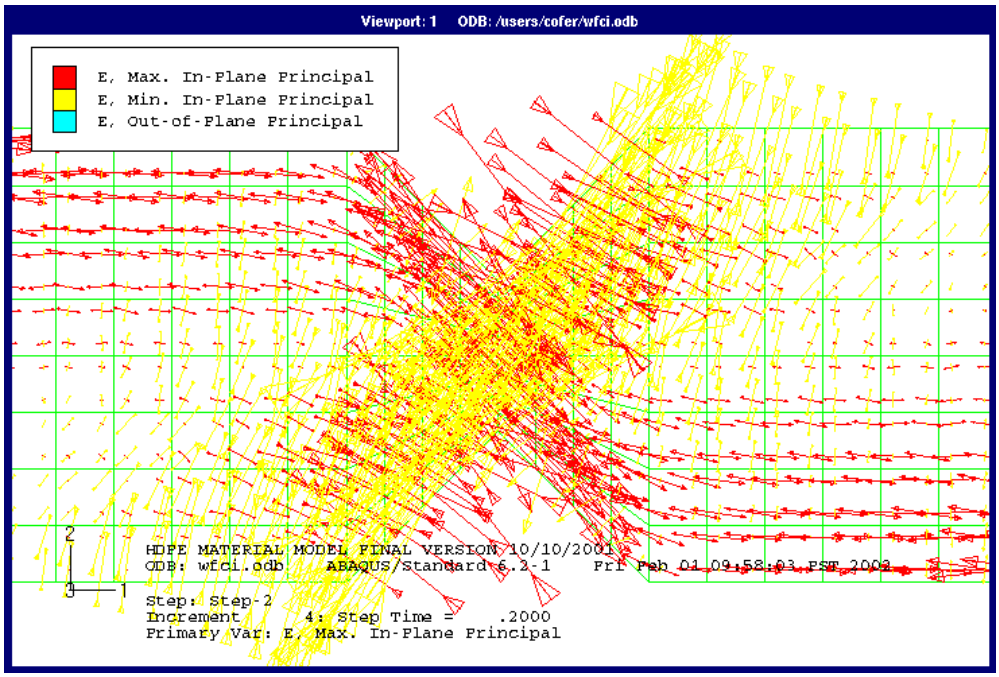

Figure 6-12: Principal strain prior to failure with isotropic damage properties

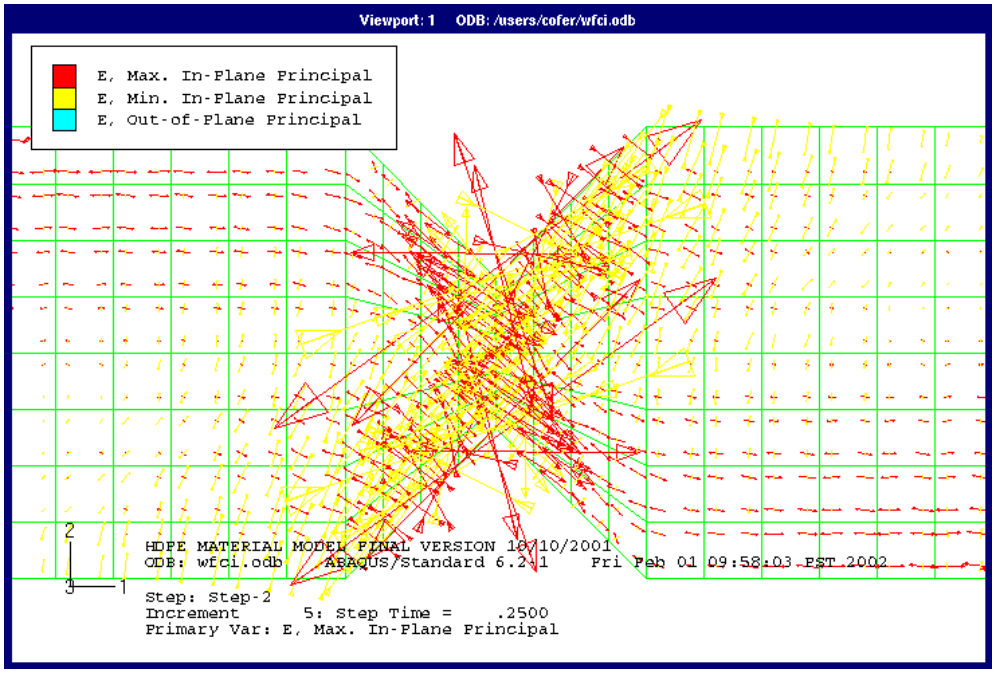

Figure 6-13: Principal strain at maximum strength with isotropic damage properties

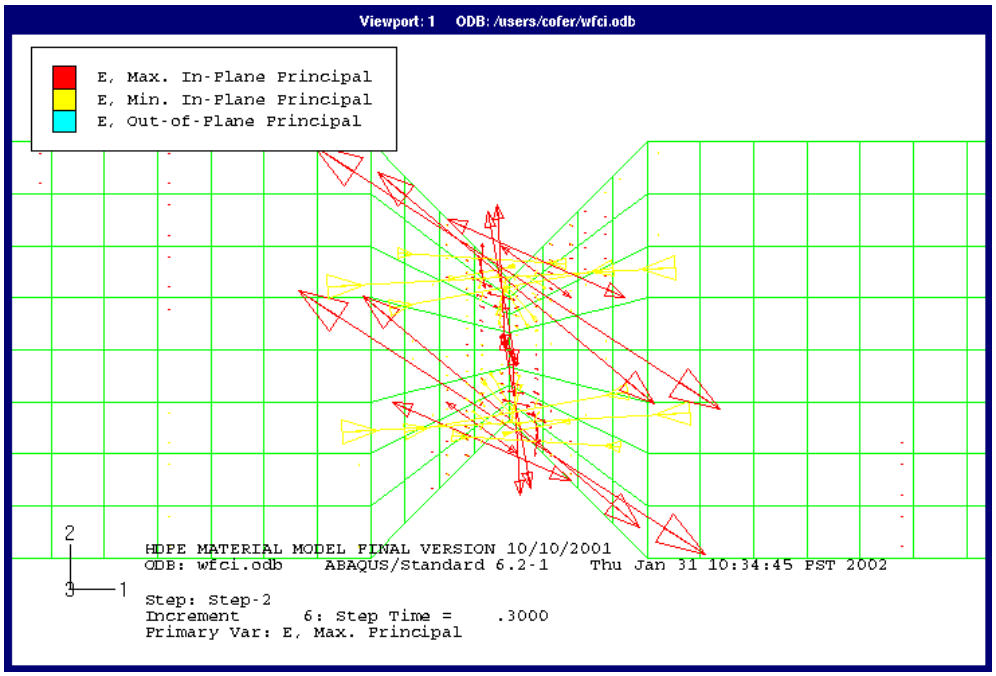

Figure 6-14: Principal strain at failure with isotropic damage properties

Maximum Iosipescu strength when failure occurs	
	Maximum Load Applied (lbs)
Finite Element Model, Orthotropic Damage	167.8
Finite Element Model, Isotropic Damage	189.4
Iosipescu Tests	146.5

Table 6-1: Comparison of the maximum strength for the material model with Iosipescu tests

6.2 Five-point beam shear bending test

Many marine fender systems are subject to bending-shear. The biaxial behavior of the HDPE material model can be investigated by modeling the five-point beam shear bending test.

The five-point bending test is used to introduce shear failure in a beam specimen. Haiar (2000) provided detailed information about this test method. Figures 6-15 and 6-16 show the test setup.

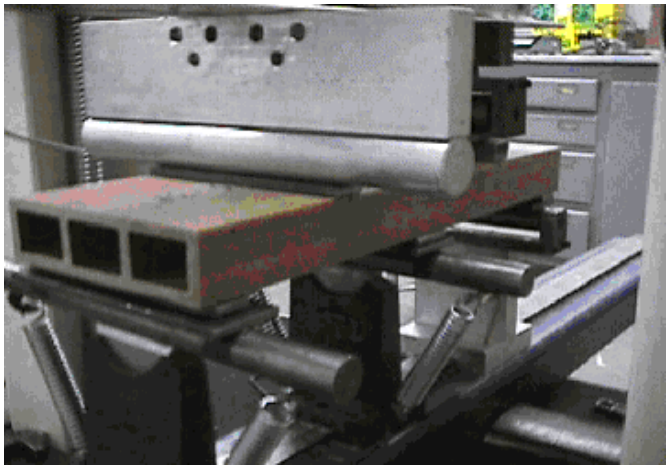

Figure 6-15: Photograph of the five-point bending shear test setup (Haiar, 2000)

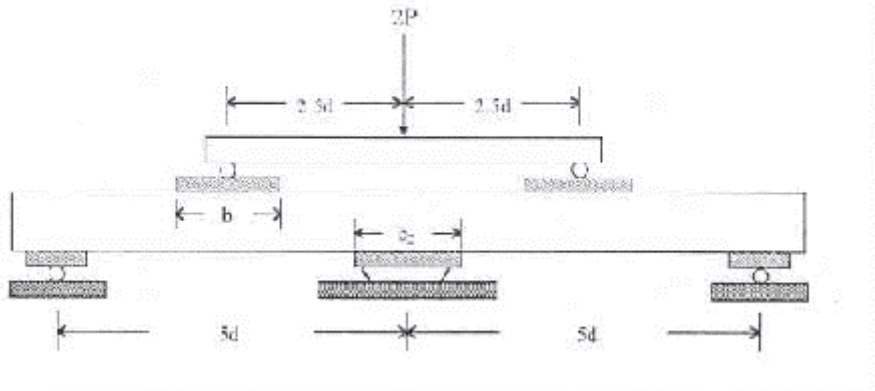

Figure 6-16: Five-point bending shear test setup (Haiar, 2000)

The five-point bending shear test model within ABAQUS finite element software is represented by Figure 6-17. As shown in the figure, the test setup is simplified as a two-dimensional beam with flanges and web, and symmetry properties were utilized. The bearing

plate was also modeled so that the model could provide similar load and support conditions to those of the test. As with the Iosipescu analysis, both orthotropic softening damage and isotropic softening damage were considered.

Load-deflection data is shown in Figure 6-18, compared with experimental results. The model and the experimental specimen both exhibited brittle behavior, with a linear response until almost the point of failure. The assumption of isotropic softening damage resulted in a significant increase in strength predicted. Numerical values are given in Table 6-2. As with Iosipescu analysis, the finite element model displayed substantially higher stiffness than the experimental specimen, most likely for the same reasons.

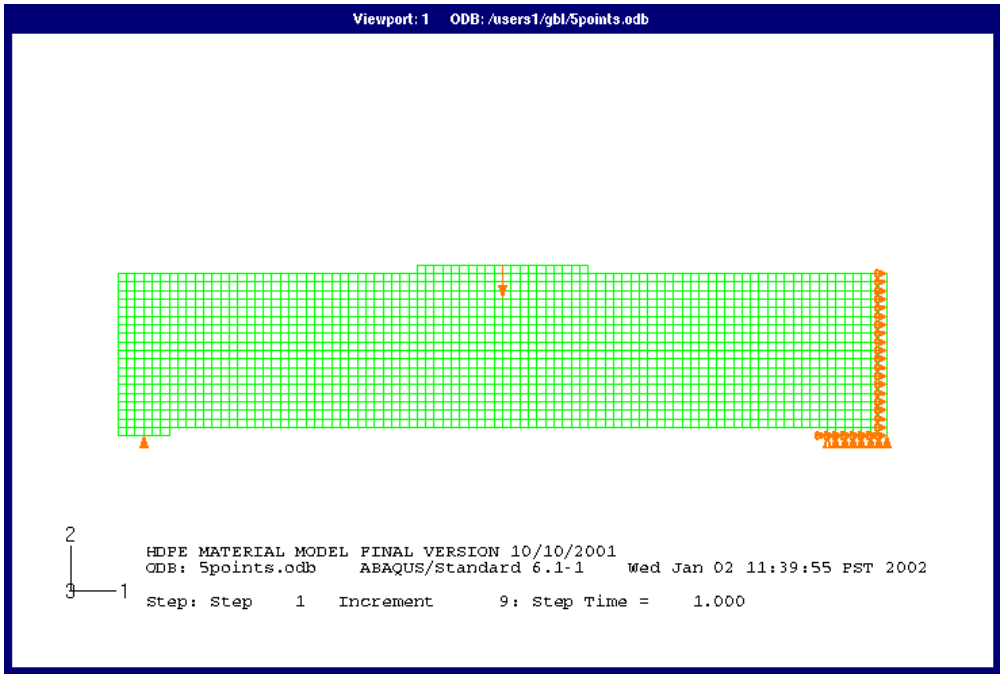

Figure 6-17: Five-point bending shear test model within ABAQUS

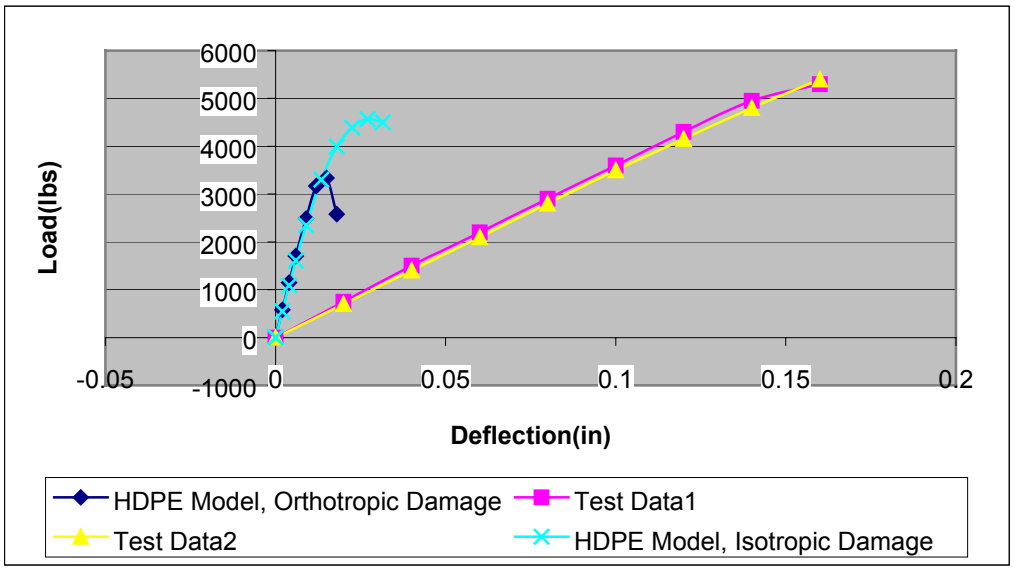

Figure 6-18: Comparison of the load-deflection relation for the five-point bending test and the HDPE material model

Maximum 5-point strength and deflection when failure occurs		
	Maximum Load applied (lbs)	Deflection (in)
Finite Element Model, Orthotropic Damage	3337	0.015
Finite Element Model, Isotropic Damage	4571	0.027
Five-point Tests	5535	0.21

Table 6-2: Comparison of the maximum strength and deflection for the material model with the five-point bending tests

Figures 6-19 and 6-20 show the softening damage parameters for the case with orthotropic damage. Note that damage for mode 1 remained identically zero and is, therefore, not shown. From the figures, the damage is caused principally by tension in mode 2, concentrated at the junction between the bottom flange and the web. The softening damage parameters for the

case of isotropic damage are shown in Figures 6-21, 6-22, and 6-23. As with the case of orthotropic damage, failure is shown to initiate between the bottom flange and the web. However, in this case, the damage occurs in both modes 1 and 2. In addition, damage in mode 2 is much more highly localized. The actual failed specimen is shown in Figure 6-24. From the photograph, failure appears to have initiated as predicted by the finite element analyses, with local failure between the bottom flange and the web, propagating in shear. Due to the localized failure displayed, the isotropic damage case appears to predict the failure mode more accurately than the orthotropic case.

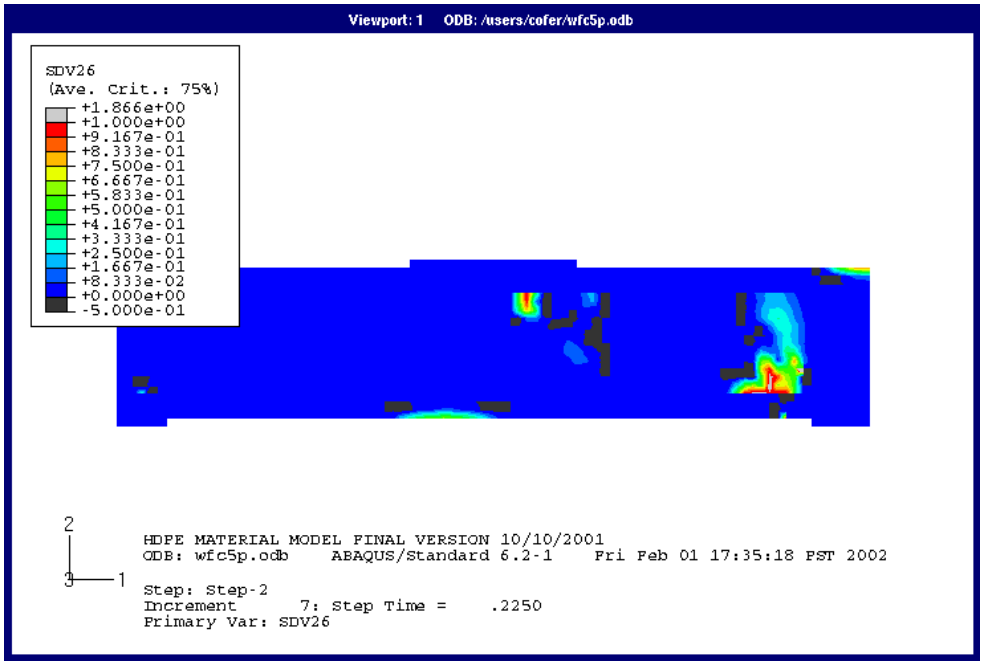

Figure 6-19: Softening damage parameter for mode 2 with orthotropic damage properties

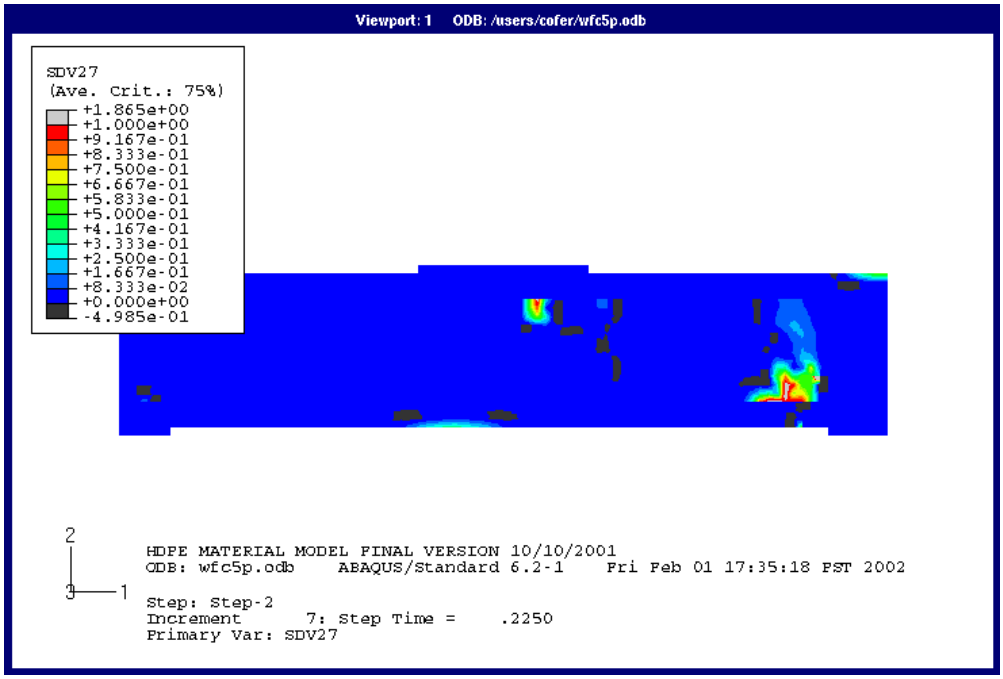

Figure 6-20: Softening damage parameter for shear with orthotropic damage properties

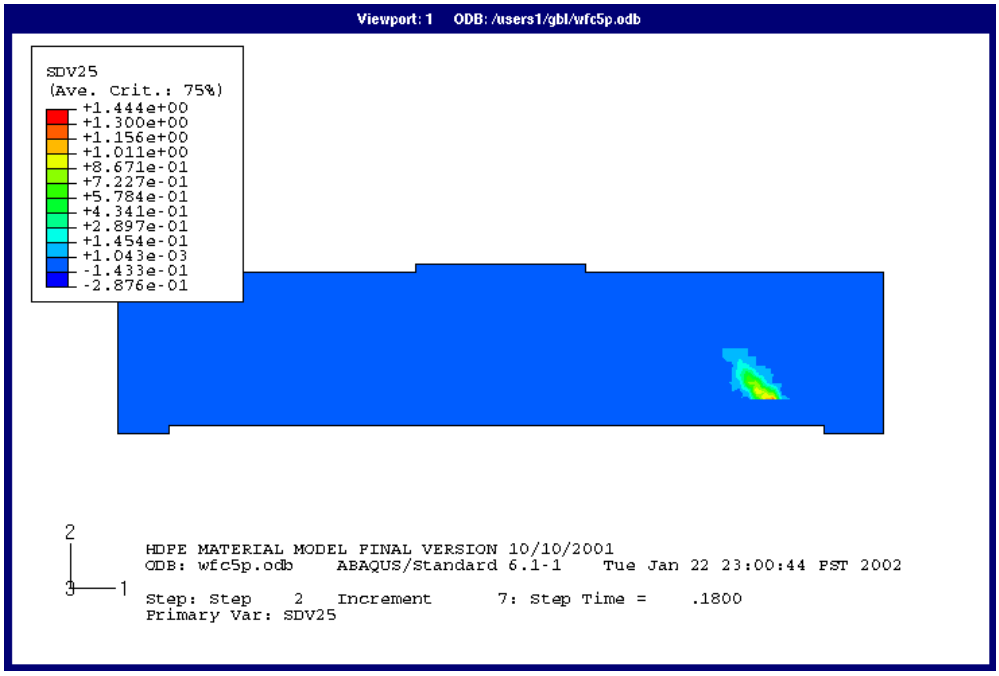

Figure 6-21: Softening damage parameter for mode 1 with isotropic damage properties

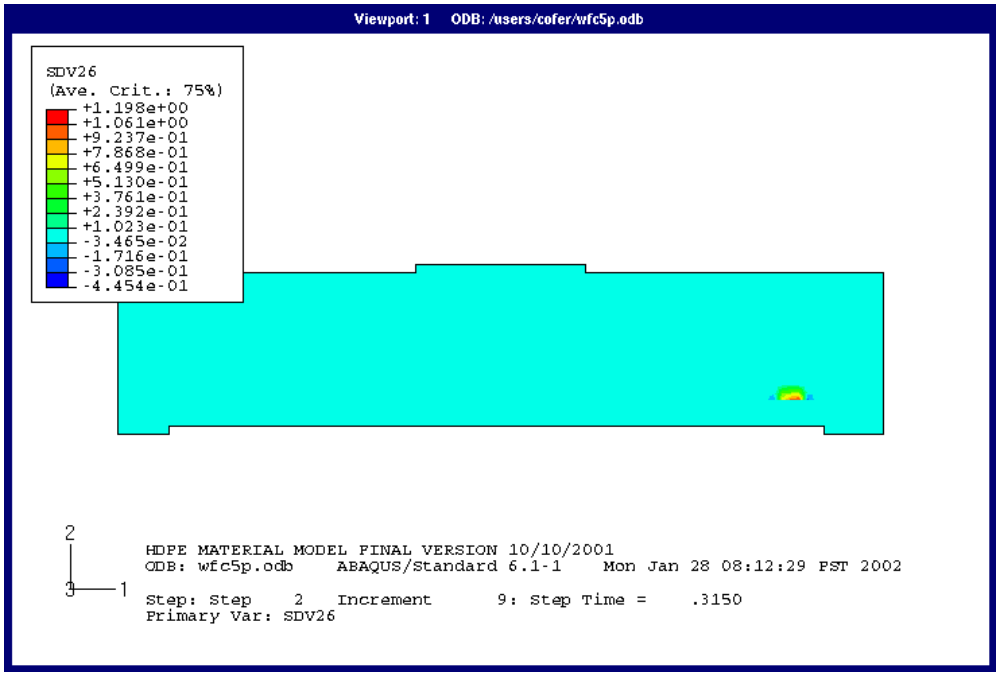

Figure 6-22: Softening damage parameter for mode 2 with isotropic damage properties

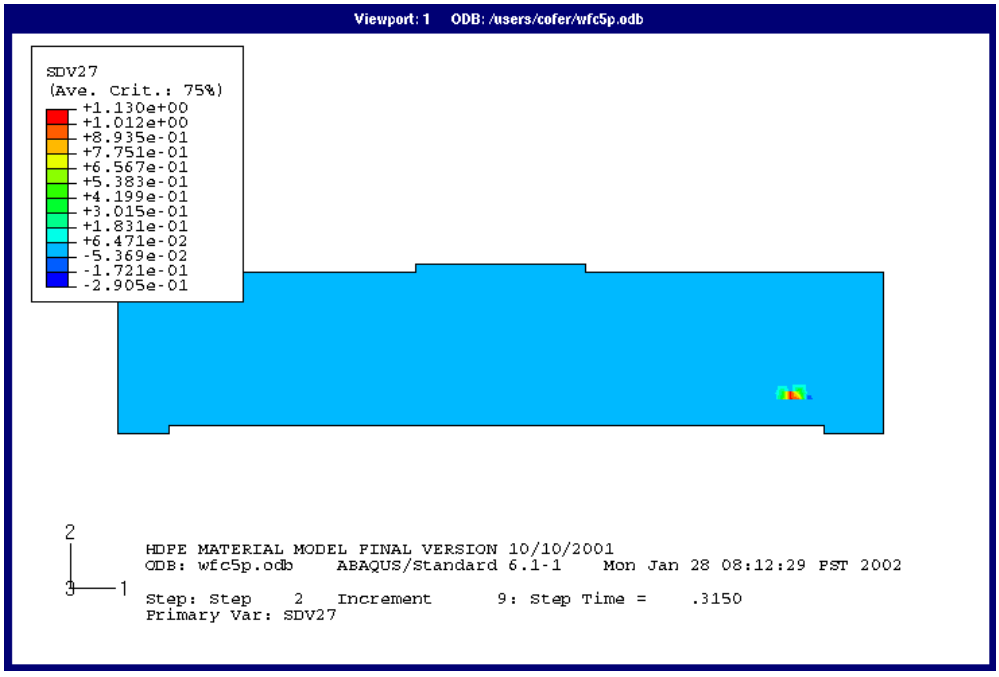

Figure 6-23: Softening damage parameter for shear with isotropic damage properties

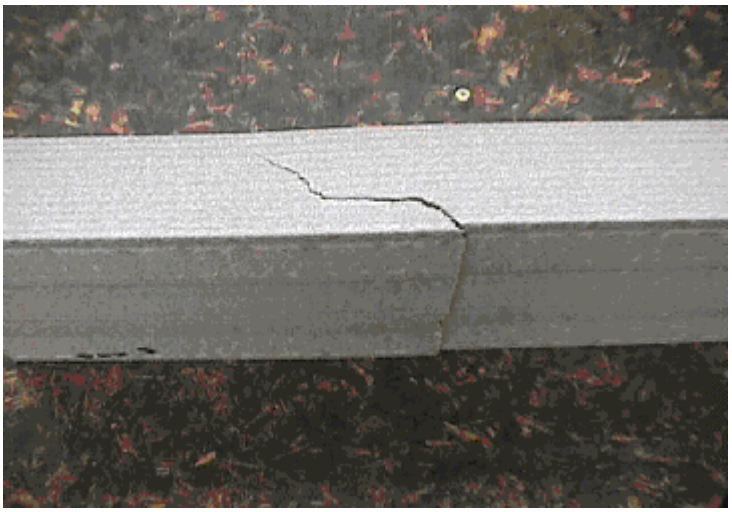

Figure 6-24: The shear failure displayed in 5-point specimen test (Haiar, 2000)

The shear strain at the point of maximum strength is shown in Figure 6-23 for the orthotropic damage case and Figure 6-24 for the isotropic damage case. In both cases, shear strain is highly localized at the point of initial failure, and its value is consistent with failure strain obtained from the torsion test of 0.022.

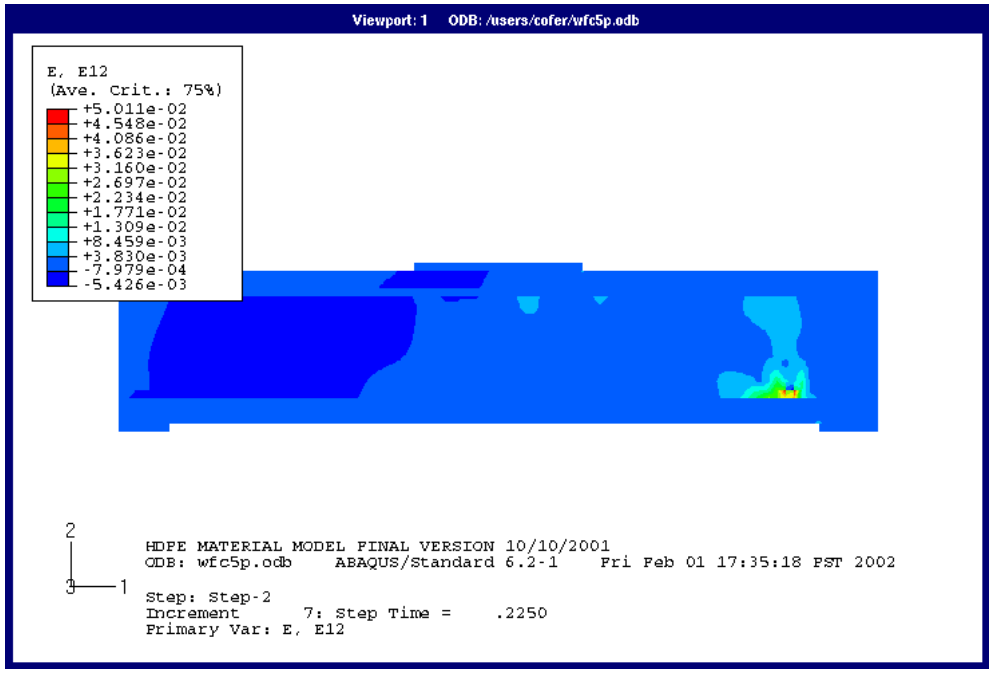

Figure 6-25: Shear strain at maximum strength with orthotropic damage properties

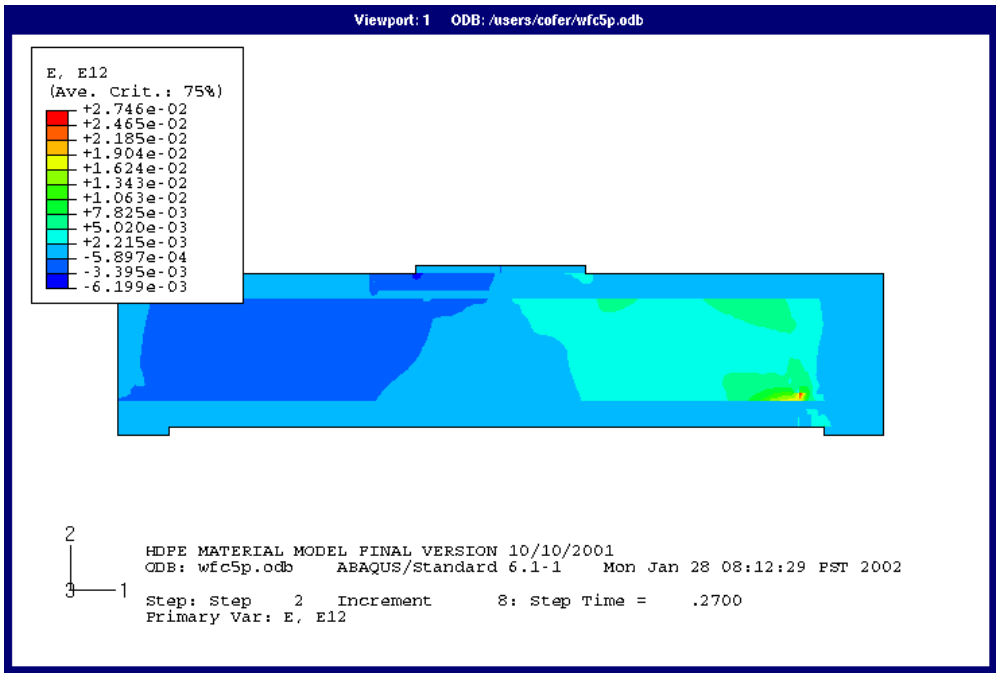

Figure 6-26: Shear strain at maximum strength with isotropic damage properties

From Table 6-2 and Figure 6-18, it is observed that the finite element model of the five-point bending shear test predicted a maximum load that is smaller than that of test results. However, the failure mode matched experimental observations, which is encouraging. From the distribution of strain and softening damage, the model with isotropic damage properties reproduced the material behavior in a more accurate way than the model with orthotropic damage properties.

6.3 Summary

Results of the Iosipescu test and the five-point bending test were presented in this chapter to evaluate the ability of the model to accurately reproduce the biaxial behavior of the HDPE wood-composite material. In both models, displacement values were substantially lower than those measured in tests. This may be a result of local crushing effects, flexibility within the test fixtures, or a lack of agreement between displacements measured. For the Iosipescu test, especially, the boundary conditions and loading were difficult to reproduce. It was shown from the five-point strain and damage contours that, like the photo of the specimen shown, when the specimen reaches the failure limit, there is an in-plane region having the same shape as the cracks in the real specimen. In addition, the failure load values were fairly close to experiment, with that from the Iosipescu test being higher and that from the five-point test being lower.

CHAPTER 7

Conclusion

In this thesis, a new material model for HDPE wood-plastic material is presented. Briefly, it can be noticed that three important components were used to realize the objectives of the material model. The first is the concept of effective stress, which is used to build the link between the damaged state and undamaged state of a material point. The second is the idea of the decomposition of the elastic tensor, which is used as a means to include the effect of anisotropy. Three modes were decomposed from the plane stress tensor used within the two-dimensional HDPE material model. Finally, the hyperbolic-tangent shape of the HDPE stress-strain relations is the basis of this material model. Based upon the shape similarity of the stress-strain relations obtained from different tests, the assumption was made that damage caused the nonlinearity of the HDPE material. From the hyperbolic-tangent shape, damage was derived in the form of a scalar, and each damage variable was set to correspond to an eigenmode derived from elastic tensor decomposition. The assumption was made that the first two eigenmodes could be related to the uniaxial behavior of the HDPE material and that the shear mode behavior is influenced by the two normal eigenmodes.

Separate damage variables were used for tension strain and compression strain within each eigenmode of the material model, by which material anisotropy in tension and compression could be modeled, as displayed in tests. The idea of volumetric strain was used to distinguish whether an eigenmode at a material point is in tension or in compression. The constitutive

relation takes the form of a function of damage to describe nonlinear stress-strain relations. The failure criteria of the HDPE material are proposed as strain-based.

Although the basic derivations were based on energy concepts, the material model was adjusted to better match experimental behavior. First, separate damage parameters for each mode were introduced to allow both material nonlinearity and softening/failure. Also, a means to define damage in the shear mode in terms of damage in the normal modes was devised. Finally, a scheme to relate damage in the normal modes to shear strain was implemented.

After implementing the theory of the material model into the finite element software ABAQUS with user subroutine UMAT, small uniaxial models were analyzed for comparison with tests. The results indicated that the use of tensile properties from tests in the direction perpendicular to extrusion, which showed very brittle behavior compared to other directions, did not lead to a consistent failure mode in the case of pure shear, which indicated nearly isotropic behavior. Thus, for all subsequent analyses, both orthotropic and isotropic damage cases were considered. In general, the isotropic cases yielded more accurate results than the orthotropic cases.

Iosipescu shear and five-point bending tests were also modeled by the use of this material model. The load-deflection curves of the Iosipescu and five-point model results indicated that the finite element model was quite stiff in comparison with experimental results. However, because stiffness of the simple uniaxial models closely matched experimental data, the apparent differences in stiffness for the complicated tests are thought to result from issues of load application and support in the models. The specimen strength values predicted in the models were fairly close to those of experiment and the failure modes were similar.

The work of this thesis raised several questions and pointed to the need for further research. Currently, the material model has no provision for reversal of strain. Even for monotonic loading, local areas of a finite element model will unload as other areas soften and fail. Also, logic needs to be introduced to consider cases in which, at an eigenmode for a material point, the strain changes from tension to compression or vice versa.

The use of volumetric strain to indicate whether the state of strain for an eigenmode is tensile or compressive needs to be investigated further. The idea was to use a strain invariant. Another possibility would be to consider principal strain values. Similarly, the logic used to assign damage to eigenmodes 1 and 2 on the basis of shear strain seemed to work reasonably well in spite of the fact that it violates the assumption that the eigenmodes do not interact. Interestingly, Arramon, et al. (2000) augmented the failure surface for their material model with a provision for principal stress. Perhaps, a condition on principal strain could be devised to better consider the interaction of shear and damage.

The performance of this material model in biaxial states of strain has not been tested conclusively due to the lack of biaxial test data. With such data, a failure surface in stress space could be plotted, evaluated, and compared to those of other materials and material models, leading to more definite conclusions.

APPENDIX A

Analysis Models and Numerical Data

•Uniaxial load - monotonically increased displacement

–x-direction
–y-direction

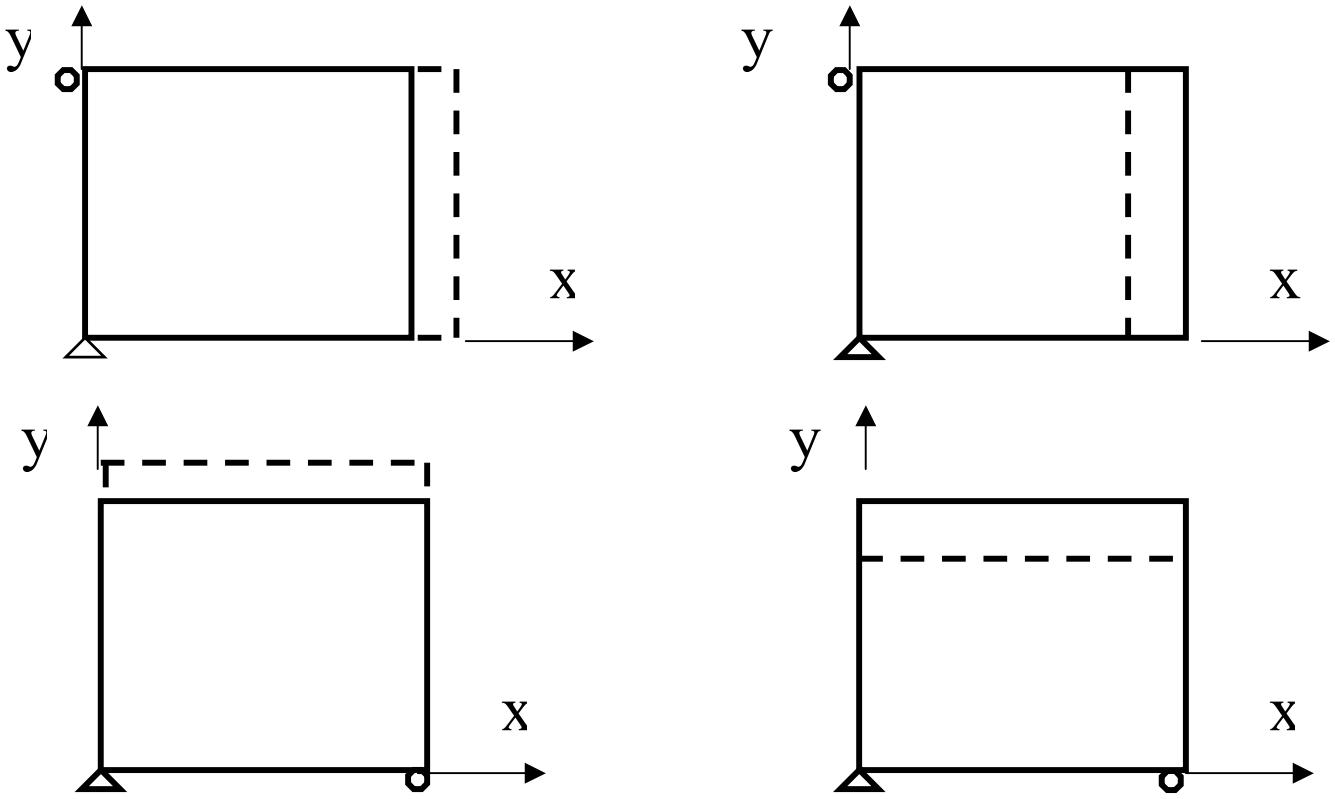

Uniaxial tension parallel to grain	
Stress (psi)	Strain(in/in)
0	0
293	6.00E-04
590	1.20E-03
918	2.10E-03
1151	3.45E-03
1211	5.48E-03
1214	8.51E-03
1214	1.31E-02
1214	1.99E-02
3	3.00E-02

Table A-1: Abaqus stress-strain results with uniaxial tension parallel to grain

Uniaxial compression parallel to grain			
Strain (in/in)	Stress (psi) Orthotropic Damage	Stress (psi) Isotropic Damage	Stress (psi) Confined with Isotropic Damage
0	0	0	0
3.00E-07	0.1465	0.1465	0.1586
7.50E-04	299.7	299.7	327.1
1.50E-03	555.1	555.1	627.2
2.63E-03	786.7	786.7	982.7
4.31E-03	105	866	1299
6.84E-03	106.3	870.1	1486
1.06E-02	106.3	870.1	1544
1.63E-02	106.3	870.1	1550
2.49E-02	106.3	0	1550
3.00E-02	106.3	0	1031

Table A-2: Abaqus stress-strain results with uniaxial compression parallel to grain

Uniaxial tension perpendicular to grain	
Stress (psi)	Strain(in/in)
0	0
0.1143	3.00E-07
86.69	1.25E-04
172.8	2.50E-04
299.8	4.38E-04
481.8	7.19E-04
725.5	1.14E-03
1006	1.77E-03
1241	2.72E-03
1261	4.15E-03
197.3	5.00E-03

Table A-3: Abaqus stress-strain results with uniaxial tension perpendicular to grain

Uniaxial compression perpendicular to grain	
Strain (in/in)	Stress (psi)
0	0
5.00E-07	0.1904
3.13E-03	646.6
6.25E-03	1199
1.09E-02	1721
1.80E-02	1958
2.85E-02	1986
4.43E-02	1987
6.81E-02	1986
1.04E-01	440.6
1.25E-01	343

Table A-4: Abaqus stress-strain results with uniaxial compression perpendicular to grain

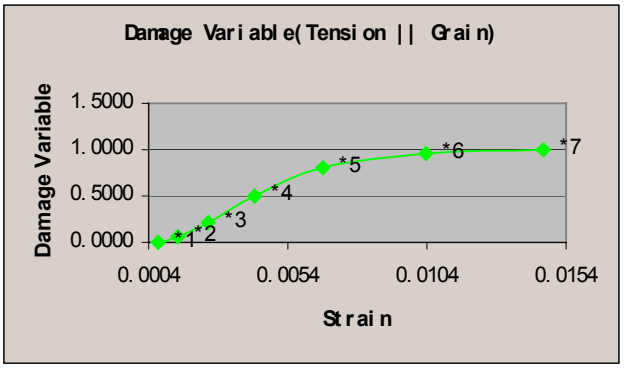

Notation:

*1. Damage variable =0.00. The initial constitutive matrix. $\underline{\underline{C}} = \begin{bmatrix} 4.45\times10^{5} & -1.70\times10^{4} & 0 \\ -1.70\times10^{4} & 5.83\times10^{4} & 0 \\ 0 & 0 & 7.49\times10^{4} \end{bmatrix}$.

*2. Damage variable =0.063. The constitutive matrix $\underline{\underline{C}} = \begin{bmatrix} 3.91\times10^{5} & -1.74\times10^{4} & 0 \\ -1.74\times10 & 5.83\times10^{4} & 0 \\ 0 & 0 & 7.02\times10^{4} \end{bmatrix}$.

*3. Damage variable =0.224. The constitutive matrix $\underline{\underline{C}} = \begin{bmatrix} 2.71\times105 & -1.84\times10^{4} & 0 \\ -1.84\times10^{4} & 5.83\times10^{4} & 0 \\ 0 & 0 & 5.81\times10^{4} \end{bmatrix}$.

*4. Damage variable =0.514. The constitutive matrix $\underline{\underline{C}} = \begin{bmatrix} 1.11\times10^{5} & -1.97\times10^{5} & 0 \\ -1.97\times10^{5} & 5.82\times10^{4} & 0 \\ 0 & 0 & 3.65\times10^{4} \end{bmatrix}$.

*5. Damage variable =0.813. The constitutive matrix $\underline{\underline{C}} = \begin{bmatrix} 2.26\times10^{4} & -2.04\times10^{4} & 0 \\ -2.04\times10^{4} & 5.82\times10^{4} & 0 \\ 0 & 0 & 1.40\times10^{4} \end{bmatrix}$.

*6. Damage variable =0.964. The constitutive matrix $\underline{\underline{C}} = \begin{bmatrix} 7.82\times10^{3} & -2.06\times10^{4} & 0 \\ -2.06\times10^{4} & 5.82\times10^{4} & 0 \\ 0 & 0 & 2.01\times10^{2} \end{bmatrix}$.

*7. Damage variable =1.000. The constitutive matrix $\underline{\underline{C}} = \begin{bmatrix} 7.26\times10^{3} & -2.06\times10^{4} & 0 \\ -2.06\times10^{4} & 5.82\times10^{4} & 0 \\ 0 & 0 & 2.01\times10^{2} \end{bmatrix}$.

Table A-9: The constitutive matrix corresponding to different damage levels (Uniaxial Tension Parallel to Grain)

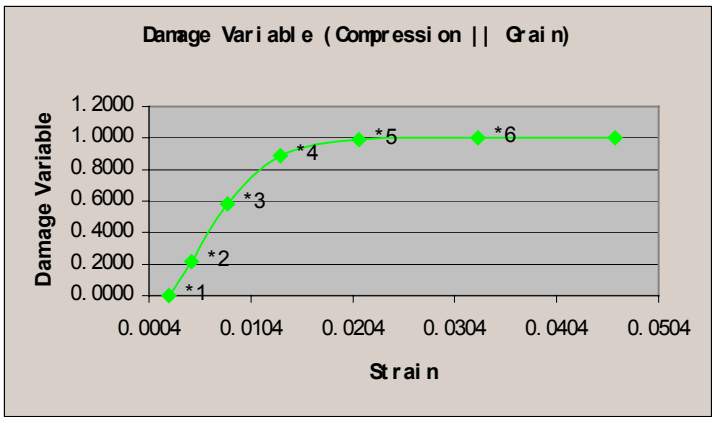

Notation:

*1. Damage variable =0.00. The initial constitutive matrix.	$\underline{\underline{C}} = \begin{bmatrix} 4.45\times10^{5} & -1.70\times10^{4} & 0 \\ -1.70\times10^{4} & 5.83\times10^{4} & 0 \\ 0 & 0 & 7.49\times10^{4} \end{bmatrix}$.
*2. Damage variable =0.4380. The constitutive matrix	$\underline{\underline{C}} = \begin{bmatrix} 1.46\times10^{5} & -1.94\times10^{4} & 0 \\ -1.94\times10^{4} & 5.82\times10^{4} & 0 \\ 0 & 0 & 4.21\times10^{4} \end{bmatrix}$.
*3. Damage variable =0.8474. The constitutive matrix	$\underline{\underline{C}} = \begin{bmatrix} 1.75\times10^{4} & -2.05\times10^{4} & 0 \\ -2.05\times10^{4} & 5.82\times10^{4} & 0 \\ 0 & 0 & 1.14\times10^{4} \end{bmatrix}$.
*4. Damage variable =0.9849. The constitutive matrix	$\underline{\underline{C}} = \begin{bmatrix} 7.35\times10^{3} & -2.06\times10^{4} & 0 \\ -2.06\times10^{4} & 5.82\times10^{4} & 0 \\ 0 & 0 & 1.14\times10^{4} \end{bmatrix}$.
*5. Damage variable =0.9996. The constitutive matrix	$\underline{\underline{C}} = \begin{bmatrix} 7.25\times10^{3} & -2.06\times10^{4} & 0 \\ -2.06\times10^{4} & 5.82\times10^{4} & 0 \\ 0 & 0 & 31.6 \end{bmatrix}$.
*6. Damage variable =1.000. The constitutive matrix	$\underline{\underline{C}} = \begin{bmatrix} 7.25\times10^{3} & -2.06\times10^{4} & 0 \\ -2.06\times10^{4} & 5.82\times10^{4} & 0 \\ 0 & 0 & 14.6 \end{bmatrix}$.

Table A-9: The constitutive matrix corresponding to different damage levels
(Uniaxial Compression Perpendicular to Grain)

APPENDIX B

ABAQUS User Subroutine
For the HDPE Material Model

HDPE MATERIAL MODEL

MACRO FLOW CHART OF THE UMAT SUBROUTINE

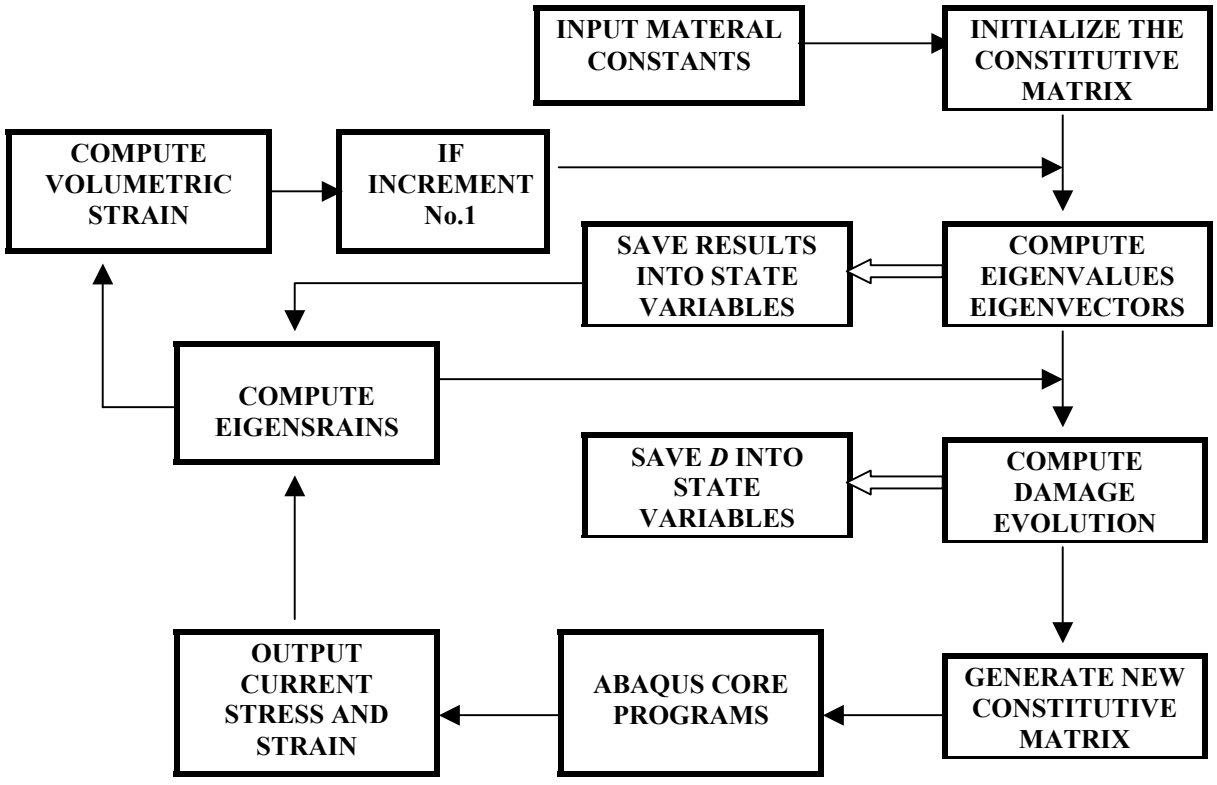

Figure B-1: Macro flow chart of the UMAT subroutine for the HDPE material model

UMAT User Subroutine for the HDPE Material Model:

```
SUBROUTINE UMAT(STRESS,STATEV,DDSDDE,SSE,SPD,SCD,
     1 RPL,DDSDDT,DRPLDE,DRPLDT,STRAN,DSTRAN,
     2 TIME,DTIME,TEMP,DTEMP,PREDEF,DPRED,MATERL,NDI,NSHR,NTENS,
     3 NSTATV,PROPS,NPROPS,COORDS,DROT,PNEWDT,CELENT,
     4 DFGRD0,DFGRD1,NOEL,NPT,KSLAY,KSPT,KSTEP,KINC)
C
      INCLUDE 'ABA_PARAM.INC'
C
      CHARACTER*80 MATERL
      DIMENSION STRESS(NTENS),STATEV(NSTATV),
     1 DDSDDE(NTENS,NTENS),DDSDDT(NTENS),DRPLDE(NTENS),
     2 STRAN(NTENS),DSTRAN(NTENS),TIME(2),PREDEF(1),DPRED(1),
     3 PROPS(NPROPS),COORDS(3),DROT(3,3),
     4 DFGRD0(3,3),DFGRD1(3,3),DSTRS(NTENS),TOTSTN(NTENS)

      DIMENSION EIVEC1(3),EIVEC2(3),EIVEC3(3),EV(3)
      DIMENSION P1(3,3),P2(3,3),P3(3,3)
      DIMENSION EISTN(3,3),SCASTN(3)
C WFC
      DIMENSION DEISTN(3,3),T(3,3),DT(3,3)
C WFC

C ------------------------------------------------------------
C     UMAT FOR SPECIFIED ORTHTROPIC MATERIAL COMPOSITE
C     CAN ONLY BE USED FOR PLANE STRESS CASES
C ------------------------------------------------------------
C     PROPS(1) - Tension a in x direction
C     PROPS(2) - Tension b in x direction
C     PROPS(3) - Compression a in x direction
C     PROPS(4) - Compression b in x direction
C     PROPS(5) - Tension a in y direction
C     PROPS(6) - Tension b in y direction
C     PROPS(7) - Compression a in y direction
C     PROPS(8) - Compression b in y direction
C     PROPS(9) - vxy
C     PROPS(10) - Tensile Strain limit in x direction
C     PROPS(11) - Compresive Strain limit in x direction
C     PROPS(12) - Tensile Strain limit in y direction
C     PROPS(13) - Compresive Strain limit in y direction
C     PROPS(14) - Shear a
C     PROPS(15) - Shear b
C     PROPS(16) - Shear Strain
C ------------------------------------------------------------
C
C     Input Elastic Properties
C
      Ax_TEN=PROPS(1)
      Bx_TEN=PROPS(2)
      Ax_COM=PROPS(3)
      Bx_COM=PROPS(4)
      Ay_TEN=PROPS(5)
      By_TEN=PROPS(6)
      Ay_COM=PROPS(7)
      By_COM=PROPS(8)
      Vxy=PROPS(9)
```

```
      a3=PROPS(14)
      b3=PROPS(15)

C
C     Damage Properties
C
      STNLxt=PROPS(10)
      STNLxc=PROPS(11)
      STNLyt=PROPS(12)
      STNLyc=PROPS(13)
      D1=STATEV(1)
      D2=STATEV(2)
      D3=STATEV(3)
      d1wfc=statev(25)
      d2wfc=statev(26)
      d3wfc=statev(27)
      stnlxtf=1.5*stnlxt
      stnlxcf=1.5*stnlxc
      stnlytf=1.2*stnlyt
      stnlycf=1.5*stnlyc
      dd1wfc=0.
      dd2wfc=0.
      dd3wfc=0.
      D1NEW=D1
      D2NEW=D2
      D3NEW=D3
      DD1=0.
      DD2=0.
      DD3=0.

C
C     Define Elastic Properties According to Strain State
C
         DO II=1,NTENS
         TOTSTN(II)=STRAN(II)+DSTRAN(II)
         END DO

       STNx=STATEV(4)
       STNy=STATEV(5)
       STNxy=STATEV(6)
       DSTNx=DSTRAN(1)
       DSTNy=DSTRAN(2)
       DSTNxy=DSTRAN(3)
C      STRx=STATEV(19)
C      STRy=STATEV(20)
C      STRxy=STATEV(21)
      VMSTN1=STATEV(14)
      VMSTN2=STATEV(15)
      STATEV(7)=STATEV(7)+1.0

      IF (STATEV(7).EQ.1.0) THEN
        a1=(Ax_COM+Ax_TEN)/2.0
        a2=(Ay_COM+Ay_TEN)/2.0
        Ex=(Ax_COM*Bx_COM+Ax_TEN*Bx_TEN)/2.0
        Ey=(Ay_COM*By_COM+Ay_TEN*By_TEN)/2.0

        ELSE IF(STATEV(7).EQ.2.0) THEN
```

```
       IF (VMSTN1.GT.1.e-8) THEN
      a1=Ax_TEN
        Ex=Ax_TEN*Bx_TEN
        STNL1=STNLxt
        stnl1f=stnlxtf
        STATEV(8)=Ex
        STATEV(9)=a1
        STATEV(10)=STNL1
        statev(28)=stnl1f
C
        ELSE
         a1=Ax_COM
         Ex=Ax_COM*Bx_COM
         STNL1=STNLxc
         stnl1f=stnlxcf
        STATEV(8)=Ex
         STATEV(9)=a1
         STATEV(10)=STNL1
         statev(28)=stnl1f
        ENDIF
C
         IF (VMSTN2.GT.1.e-8) THEN
          a2=Ay_TEN
          Ey=Ay_TEN*By_TEN
          STNL2=STNLyt
          stnl2f=stnlytf
          STATEV(11)=Ey
          STATEV(12)=a2
          STATEV(13)=STNL2
          statev(29)=stnl2f
        ELSE
        a2=Ay_COM
        Ey=Ay_COM*By_COM
        STNL2=STNLyc
        stnl2f=stnlycf
        STATEV(11)=Ey
        STATEV(12)=a2
        STATEV(13)=STNL2
        statev(29)=stnl2f
        ENDIF

      ELSE
      Ex=STATEV(8)
      a1=STATEV(9)
      STNL1=STATEV(10)
      stnl1f=statev(28)
      Ey=STATEV(11)
      a2=STATEV(12)
      STNL2=STATEV(13)
      stnl2f=statev(29)

      ENDIF


      Gxy=a3*b3
      Vyx=Ey*Vxy/Ex
```

```
C -------------------------------------------------------------
C    CACULATE EIGENVALUES AND EIGENVECTORS
C -------------------------------------------------------------

       TERM1=1.0/(1.0-Vxy*Vyx)
       C11=Ex*TERM1
       C12=Vxy*Ex*TERM1
       C21=Vyx*Ey*TERM1
       C22=Ey*TERM1
       C66=Gxy

       EV(3)=2*C66
       EV(1)=(C22+C11+SQRT(C22**2+C11**2-2*C11*C22+4*C12*C21))/2.0
       EV(2)=(C22+C11-SQRT(C22**2+C11**2-2*C11*C22+4*C12*C21))/2.0

       TEMP0=-C12/(C11-EV(1))
       TEMP1=SQRT((-C12/(C11-EV(1)))**2+1.0)
       TEMP2=-C12/(C11-EV(2))
       TEMP3=SQRT((-C12/(C11-EV(2)))**2+1.0)
       EIVEC1(1)=TEMP0/TEMP1
       EIVEC1(2)=1./TEMP1
       EIVEC1(3)=0.

       EIVEC2(1)=TEMP2/TEMP3
       EIVEC2(2)=1./TEMP3
       EIVEC2(3)=0.

       EIVEC3(1)=0.
       EIVEC3(2)=0.
       EIVEC3(3)=1.


C-----------------------------------------------
C     DAMAGE EVOLUTION
C     SCASTN(I)------SCALAR STRAIN
C     DDx--------DAMAGE INCREMENT FOR MODE X
C-----------------------------------------------

      DO I=1,3
      EISTN(1,I)=0.
      EISTN(2,I)=0.
      EISTN(3,I)=0.
      DEISTN(1,I)=0.
      DEISTN(2,I)=0.
      DEISTN(3,I)=0.
      T(1,I)=0.
      T(2,I)=0.
      T(3,I)=0.

      SCASTN(I)=0.
      END DO

      DO I=1,3
       DO J=1,3
        P1(I,J)=0.
```

```
        P2(I,J)=0.
        P3(I,J)=0.
       END DO
      END DO

      DO I=1,3
       DO J=1,3
        P1(I,J)=P1(I,J)+EIVEC1(I)*EIVEC1(J)
        P2(I,J)=P2(I,J)+EIVEC2(I)*EIVEC2(J)
        P3(I,J)=P3(I,J)+EIVEC3(I)*EIVEC3(J)
       END DO
      END DO

      DO I=1,3
      EISTN(1,I)=EISTN(1,I)+P1(I,1)*STNx
     + +P1(I,2)*STNy+P1(I,3)*STNxy*1.414213562
      EISTN(2,I)=EISTN(2,I)+P2(I,1)*STNx
     + +P2(I,2)*STNy+P2(I,3)*STNxy*1.414213562
      EISTN(3,I)=EISTN(3,I)+P3(I,1)*STNx
     + +P3(I,2)*STNy+P3(I,3)*STNxy*1.414213562
      DEISTN(1,I)=DEISTN(1,I)+P1(I,1)*DSTNx
     + +P1(I,2)*DSTNy+P1(I,3)*DSTNxy*1.414213562
      DEISTN(2,I)=DEISTN(2,I)+P2(I,1)*DSTNx
     + +P2(I,2)*DSTNy+P2(I,3)*DSTNxy*1.414213562
      DEISTN(3,I)=DEISTN(3,I)+P3(I,1)*DSTNx
     + +P3(I,2)*DSTNy+P3(I,3)*DSTNxy*1.414213562

      END DO

      T(1,1)=STATEV(16)
      T(1,2)=STATEV(17)
      T(1,3)=STATEV(18)
      T(2,1)=STATEV(19)
      T(2,2)=STATEV(20)
      T(2,3)=STATEV(21)
      T(3,1)=STATEV(22)
      T(3,2)=STATEV(23)
      T(3,3)=STATEV(24)

C      WRITE(6,'(3E12.5)')STNx, STNy, STNxy
C      write (6,*) 'stress ',stress(1),stress(2),stress(3)
C      write (6,*) 'T, 1', t(1,1),t(2,1),t(3,1)
C      write (6,*) 'T, 2',t(1,2),t(2,2),t(3,2)
C      write (6,*) 'T, 3',t(1,3),t(2,3),t(3,3)

      VMSTN1=EISTN(1,1)+EISTN(1,2)+EISTN(1,3)
      VMSTN2=EISTN(2,1)+EISTN(2,2)+EISTN(2,3)
      dvmstn1=deistn(1,1)+deistn(1,2)+deistn(1,3)
      dvmstn2=deistn(2,1)+deistn(2,2)+deistn(2,3)
      IF(VMSTN1.GT.-1.E-8) THEN
      STATEV(14)=1.0
      ELSE
      STATEV(14)=0.
      ENDIF
      IF(VMSTN2.GT.-1.E-8) THEN
      STATEV(15)=1.0
      ELSE
```

```
STATEV(15)=0.
ENDIF

DO I=1,3
SCASTN(1)=SCASTN(1)+EISTN(1,I)*EISTN(1,I)
SCASTN(2)=SCASTN(2)+EISTN(2,I)*EISTN(2,I)
SCASTN(3)=SCASTN(3)+EISTN(3,I)*EISTN(3,I)
END DO

DO I=1,3
SCASTN(I)=SQRT(SCASTN(I))
END DO

IF (SCASTN(1).LE.1E-8.AND.SCASTN(2).LE.1E-8) THEN
SCASTN(1)=SCASTN(3)*1.0/2.
SCASTN(2)=SCASTN(3)*1.0/2.
STATEV(14)=1.0
STATEV(15)=0.
ELSE
SCASTN(1)=SCASTN(1)+SCASTN(3)*1.0/2.
SCASTN(2)=SCASTN(2)+SCASTN(3)*1.0/2.
END IF


  D1NEW=1-(1/COSH(EV(1)*SCASTN(1)/a1))**2
  IF (D1NEW.GT.1.) THEN
  D1NEW=1.0
  ENDIF
  DD1=D1NEW-D1
  STATEV(1)=D1NEW
  IF (DD1.LT.0.) DD1=0.

  if (abs(scastn(1)).gt.stnl1) then
    d1wfcnew=(abs(scastn(1))-stnl1)/(stnl1f-stnl1)
    if (d1wfcnew.gt.1.) d1wfcnew=1.
    dd1wfc=d1wfcnew-d1wfc
    statev(25)=d1wfcnew

  endif
  if (abs(scastn(2)).gt.stnl2) then
    d2wfcnew=(abs(scastn(2))-stnl2)/(stnl2f-stnl2)
    if (d2wfcnew.gt.1.) d2wfcnew=1.
    dd2wfc=d2wfcnew-d2wfc
    statev(26)=d2wfcnew

  endif

  D2NEW=1-(1/COSH(EV(2)*SCASTN(2)/a2))**2

  IF (D2NEW.GT.1.) THEN
  D2NEW=1.0
  ENDIF
  DD2=D2NEW-D2
  STATEV(2)=D2NEW
  IF (DD2.LT.0.) DD2=0.
```

```
       D3NEW=1-SQRT((1-D1NEW)*(1-D2NEW))

       IF (D3NEW.GE.1.0) THEN
       D3NEW=1.0
       ENDIF
       STATEV(3)=D3NEW
       DD3=D3NEW-D3

       d3wfcnew=1.-sqrt((1.-d1wfcnew)*(1.-d2wfcnew))
       if (d3wfcnew.gt.1.) d3wfcnew=1.
       dd3wfc=d3wfcnew-d3wfc
       statev(27)=d3wfcnew

       IF (STATEV(1).GT.1.) STATEV(1)=1.0
       IF (STATEV(2).GT.1.) STATEV(2)=1.0
       IF (STATEV(3).GT.1.) STATEV(3)=1.0
C-----------------------------------------------
C     DAMAGE INCREMENT and DAMAGE PARAMETER
C     DD---DELTA D
C-----------------------------------------------



C-----------------------------------------------
C     GENERATE NEW CONSTITUTIVE MATRIX
C-----------------------------------------------

       DO 20 K2=1,3
       DO 10 K1=1,3
           DDSDDE(K1,K2)=0.
 10    CONTINUE
 20    CONTINUE

       DDSDDE(1,1)=(1-D1NEW)*(1-D1NEW)*EV(1)*P1(1,1)
     1  +(1-D2NEW)*(1-D2NEW)*EV(2)*P2(1,1)
     2  +(1-D3NEW)*(1-D3NEW)*EV(3)*P3(1,1)
       DDSDDE(1,2)=(1-D1NEW)*(1-D1NEW)*EV(1)*P1(1,2)
     3  +(1-D2NEW)*(1-D2NEW)*EV(2)*P2(1,2)
     4  +(1-D3NEW)*(1-D3NEW)*EV(3)*P3(1,2)
       DDSDDE(2,1)=DDSDDE(1,2)
       DDSDDE(2,2)=(1-D1NEW)*(1-D1NEW)*EV(1)*P1(2,2)
     5  +(1-D2NEW)*(1-D2NEW)*EV(2)*P2(2,2)
     6  +(1-D3NEW)*(1-D3NEW)*EV(3)*P3(2,2)
       DDSDDE(3,3)=(1-D1NEW)*(1-D1NEW)*EV(1)*P1(3,3)
     7  +(1-D2NEW)*(1-D2NEW)*EV(2)*P2(3,3)
     8  +(1-D3NEW)*(1-D3NEW)*EV(3)*P3(3,3)

C--------------------------------------
C    SAVE UPDATED CONSTITUTIVE MATRIX
C    INTO STATE VARIABLES
C--------------------------------------

C
C     EIGEN STRESS INCREMENTS
C
      DO III=1,3
```

```
        DT(1,III)=(1.-D1NEW)*(1.-d1new)*EV(1)*DEISTN(1,III)
     +             -dd1wfc*t(1,iii)
        DT(2,III)=(1.-D2NEW)*(1.-d2new)*EV(2)*DEISTN(2,III)
     +             -dd2wfc*t(2,iii)
        DT(3,III)=(1.-D3NEW)*(1.-d3new)*EV(3)*DEISTN(3,III)
     +             -dd3wfc*t(3,iii)
       ENDDO
C
       DO III=1,3
C
C      SUM EIGEN STRESSES
C
         T(1,III)=T(1,III)+DT(1,III)
         T(2,III)=T(2,III)+DT(2,III)
         T(3,III)=T(3,III)+DT(3,III)


       ENDDO
       STATEV(16)=T(1,1)
       STATEV(17)=T(1,2)
       STATEV(18)=T(1,3)
       STATEV(19)=T(2,1)
       STATEV(20)=T(2,2)
       STATEV(21)=T(2,3)
       STATEV(22)=T(3,1)
       STATEV(23)=T(3,2)
       STATEV(24)=T(3,3)
C
C      TRANSFORM EIGEN STRESSES BACK TO TENSORIAL COMPONENTS
C
       DO III=1,3
         STRESS(III)=0.
       ENDDO
       DO III=1,3
         DO JJJ=1,3
           STRESS(III)=STRESS(III)+P1(III,JJJ)*T(1,JJJ)
           STRESS(III)=STRESS(III)+P2(III,JJJ)*T(2,JJJ)
           STRESS(III)=STRESS(III)+P3(III,JJJ)*T(3,JJJ)
         ENDDO
       ENDDO

C
C      Compute Current Total Strain
C
         DO II=1,NTENS
         TOTSTN(II)=STRAN(II)+DSTRAN(II)
         END DO
        STATEV(4)=TOTSTN(1)
        STATEV(5)=TOTSTN(2)
        STATEV(6)=TOTSTN(3)

        DO I=1,3
        EISTN(1,I)=0.
        EISTN(2,I)=0.
        EISTN(3,I)=0.
        END DO
```

```
        DO I=1,3
        EISTN(1,I)=EISTN(1,I)+P1(I,1)*TOTSTN(1)
      + +P1(I,2)*TOTSTN(2)+P1(I,3)*TOTSTN(3)*1.414213562
        EISTN(2,I)=EISTN(2,I)+P2(I,1)*TOTSTN(1)
      + +P2(I,2)*TOTSTN(2)+P2(I,3)*TOTSTN(3)*1.414213562
        EISTN(3,I)=EISTN(3,I)+P3(I,1)*TOTSTN(1)
      + +P3(I,2)*TOTSTN(2)+P3(I,3)*TOTSTN(3)*1.414213562
        END DO
C
        VMSTN1=EISTN(1,1)+EISTN(1,2)+EISTN(1,3)
        VMSTN2=EISTN(2,1)+EISTN(2,2)+EISTN(2,3)

        IF(VMSTN1.GT.-1.e-8) THEN
        STATEV(14)=1.0
        ELSE
        STATEV(14)=0.
        ENDIF
        IF(VMSTN2.GT.-1.e-8) THEN
        STATEV(15)=1.0
        ELSE
        STATEV(15)=0.
        ENDIF
       RETURN
       END
```

APPENDIX C

ABAQUS Input and Output File for the HDPE Material Model

Execution Procedures of Input File:

***Define nodes**

***Define type of element and element group**

***Define element section**

***Define orientation**

***Define material**
Input material constants and properties
Implement user subroutine

***Specify the number of state variables**

***Definition of step**

***Indicate type of analysis**

***Define an amplitude curve**

***Define boundary conditions**

***Set time incrementation control parameters**

***Output results**

Sample Input File

```
*HEADING
HDPE MATERIAL MODEL FINAL VERSION 10/10/2001
*RESTART, WRITE, FREQUENCY=1
*NODE
1,0.,0.,0.
2,20.,0.,0.
3,20.,20.,0.
4,0.,20.,0.
*ELEMENT, TYPE=CPS4, ELSET=WOOD_COM
1,1,2,3,4
*SOLID SECTION, ELSET=WOOD_COM, MATERIAL=HDPE
0.25
*ORIENTATION,NAME=LOCAL,SYSTEM=RECTANGULAR,DEFINITION=OFFSET TO NODES
 2, 4
*MATERIAL, NAME=HDPE
*USER MATERIAL, CONSTANTS=16
1271.,339.,2200.,213.,794.1,698.4,2284.1,119.3
0.3,0.0149,0.0459,0.00251,0.0461,1506.,87.,0.022
*DEPVAR
15

*STEP,INC=20,NLGEOM=NO
*STATIC
  0.05, 1.
*AMPLITUDE, NAME=CONSTANT
 0.,1.,1.,1.
*AMPLITUDE, NAME=VARIED
 0.,0.,1.,1.
*BOUNDARY, TYPE=DISPLACEMENT, AMPLITUDE=CONSTANT
 1,1,2
 2,2
 4,1

*BOUNDARY, TYPE=DISPLACEMENT, AMPLITUDE=VARIED
 2,1,1,-0.922
 3,1,1,-0.922


*CONTROLS, PARAMETER=TIME INCREMENTATION
*RESTART, WRITE
**
*EL PRINT, POS=INTEG, FREQ=1
 S,
 E,
*EL FILE,  POS=INTEG, FREQ=1
 S,
 E,
**NODE PRINT, FREQ=0
**  U,
**  RF,
**NODE FILE, FREQ=0
**  U,
**  RF,
```

```
**
*EL PRINT, POS=NODES, FREQ=0
**
*EL FILE,  POS=NODES, FREQ=0
**
*EL PRINT, POS=CENTR, FREQ=1
 S,
 E,
*EL FILE,  POS=CENTR, FREQ=1
 S,
 E,
*EL PRINT, POS=AVERAGE, FREQ=1
 S,
 E,
*EL FILE,  POS=AVERAGE, FREQ=1
 S,
 E,
*MODAL PRINT, FREQ=0
**
*MODAL FILE, FREQ=0
**
*ENERGY PRINT, FREQ=0
**
*ENERGY FILE, FREQ=0
**
*PRINT, FREQ=1
**
*END STEP
```

References

1. **American Society of Testing** Materials, (1998) Standard Test Method for Shear Properties of Composite Materials by the V-notched Beam Method, ASTM D5379.

2. **Arramon, Y. P., Mehrabadi, M. M., Martin D. W., Cowin, S. C.,** (2000) A Multidimentional Anistropic Strength Criterion Based on Kelvin Modes, International Journal of Solids and Structures, Pergamon Press, 37, 2915-2935.

3. **Biegler, M.W.**, **Mehrabadi, M. M.**, (1995). An energy-based constitutive model for anisotropic solids subject to damage. Mechanics of Materials, Elsevier, 19, 151-164.

4. **Caiazzo, A.A., Costanzo, F.**, (2000) On the constitutive relations of materials with evolving microstructure due to microcracking, International Journal of Solids and Structures, Pergamon Press, 37, 3375-3398.

5. **Chow, C.L., Lu, T.J.,** (1989) On evolution laws of anisotropic damage, Engineering Fracture Mechanics, Pergamon Press, 34, 679-701.

6. **Cofer, W. F., Mclean, D. I., Paynter, M. E., Wang, H.,** (1998) The Development and Verification of Finite Element Models to Optimize the design of Wale/Chock Structural Sections, Prepared for Office of Naval Research under Contract N00014-97-C-0395, 1998 Yearly Report, Washington State University, Pullman, WA.

7. **Cofer, W. F.**, **Yang, W.**, (1999) The Development and Verification of Finite Element Models to Optimize the design of Wale/Chock Structural Sections, Prepared for Office of Naval Research under Contract N00014-97-C-0395, 1999 Yearly Report, Washington State University, Pullman, WA.

8. **Coleman, B.D., Gurtin, M.E.**, (1967) Thermodynamics with Internal State Variables, Journal of Chemical Physics, 47, 597-613.

9. **Coleman, B.D., Noll, W.**, (1963) The Thermodynamics of Elastic Materials with Heat Conduction and Viscosity, Archive for Rational Mechanics and Analysis, 18, 245-261.

10. **Cowin S. C.**, **Mehrabadi, M. M.**, (1992) The Structure of The Linear Anisotropic Elastic Symmetries, J. Mech. Phys. Solids, 40.7, 1459-1471.

11. **Germain, P., Nguyen, Q.S., Suquet, P.M.**, (1983) Continuum Thermodynamics, Journal of Applied Mechanics, 50, 1010-1020.

12. **Haiar, K. J.**, (2000) Performance and Design of Prototype Wood-Plastic Composite Sections, Thesis for partial fulfillment of the degree of Master of Science, Washington State University, Pullman, WA.

13. **Lemaitre, J.**, (1983) A Continuous Damage Mechanics Model for Ductile Fracture, J. of Engineering Materials and Technology, 107, 83-89.

14. **Lockyear, S. A.**, (1999) Mechanical Analysis of Transversely Loaded Wood/Plastic sections, Thesis for partial fulfillment of the degree of Master of Science, Washington State University, Pullman, WA.

15. **Matzenmiller, A., Lubliner, J., Taylor, R.L.**, (1995) A Constitutive Model for Anisotropic Damage in Fiber-composites, Mechanics of Materials, Elsevier Science, 20, 125-152.

16. **Mehrabadi, M. M.**, **Cowin S. C.**, (1990) Eigentensors of Linear Anisotropic elastic materials, Q. J. Mech. Appl. Math., 43.1, 15-41

17. **Schreyer, H.L., Zuo, Q.H.**, (1995) Anisotropic Yield Surfaces Based on Elastic Projection Operators, J Appl. Mech., 62, 780-785.

18. **Zhu Y. and Cescotto S.,** (1995) A Fully Coupled Elastic-visco-plastic Damage Theory for Anisotropic Materials, International Jounal of Solids and Structures, 32,11, 1607-1641.